CHAPTER 3

RESULTS AND INTERPRETATION

3.1 Well log correlation to seismic data

Seven wells with good geophysical logs are in the study area. However, the logged intervals of each of these wells are not the same because not every log covers the entire interval from the base of the upper casing shoe to the total depth of the well. This is particularly so for the sonic and density logs, which are the logs needed to create a synthetic seismogram for each well.

3.1.1 Sandstone layer selection for porosity prediction

By analyzing gamma ray, resistivity, and neutron logs, two sandstone layers, sandstone 1 and sandstone 2, were selected for analysis in porosity prediction and subsequent mapping. These two layers were assumed to have potential hydrocarbon reservoirs. These sandstone layers were identified in each well. They are shown in Figures 3.1 to 3.8. The density logs of each well were transformed to density-porosity logs and have been used as target logs for attribute analysis and porosity estimation in the EMERGE®® program.

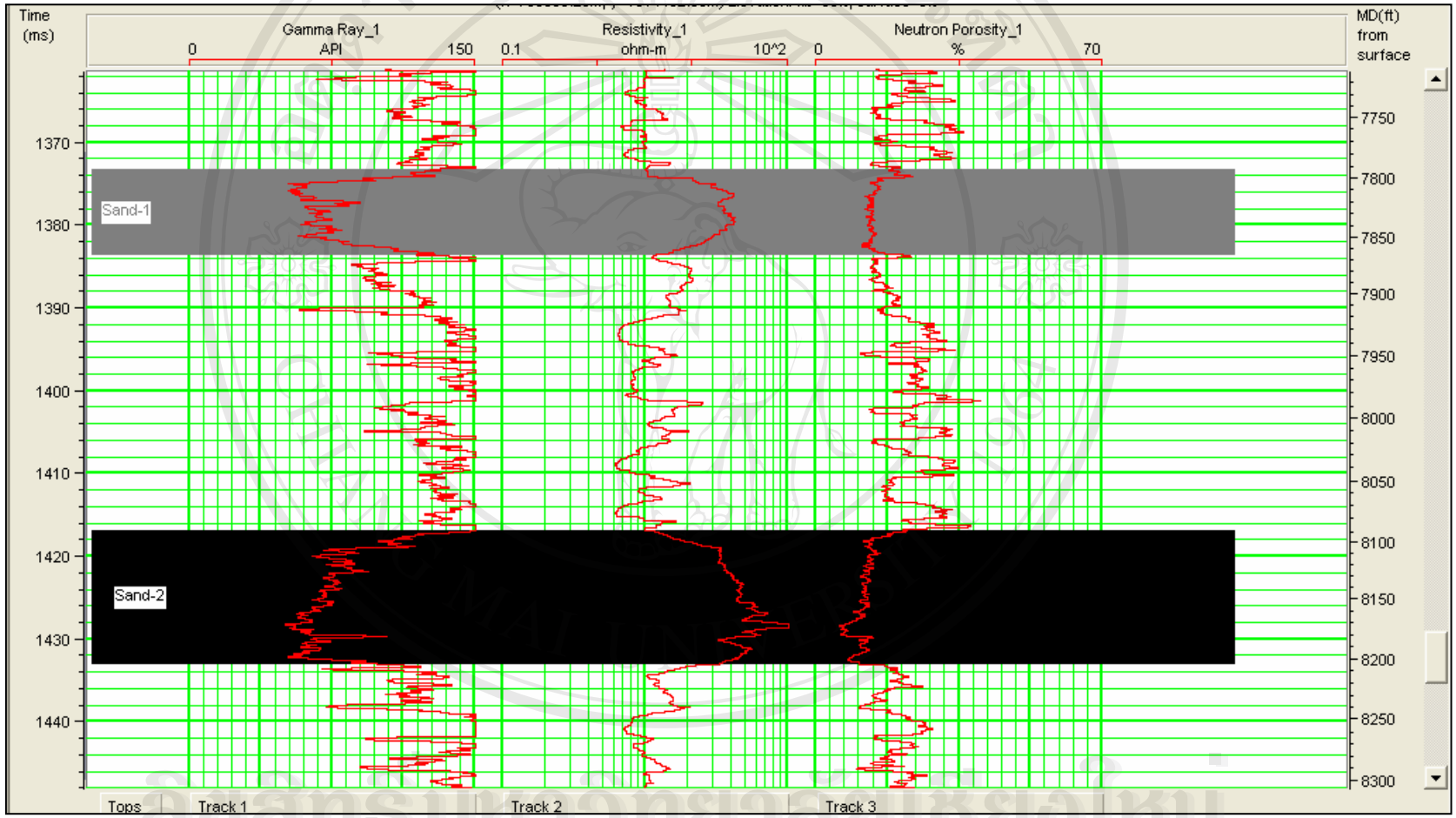

Figure 3.1 Target sandstone layers 1 and 2 in Well-1.

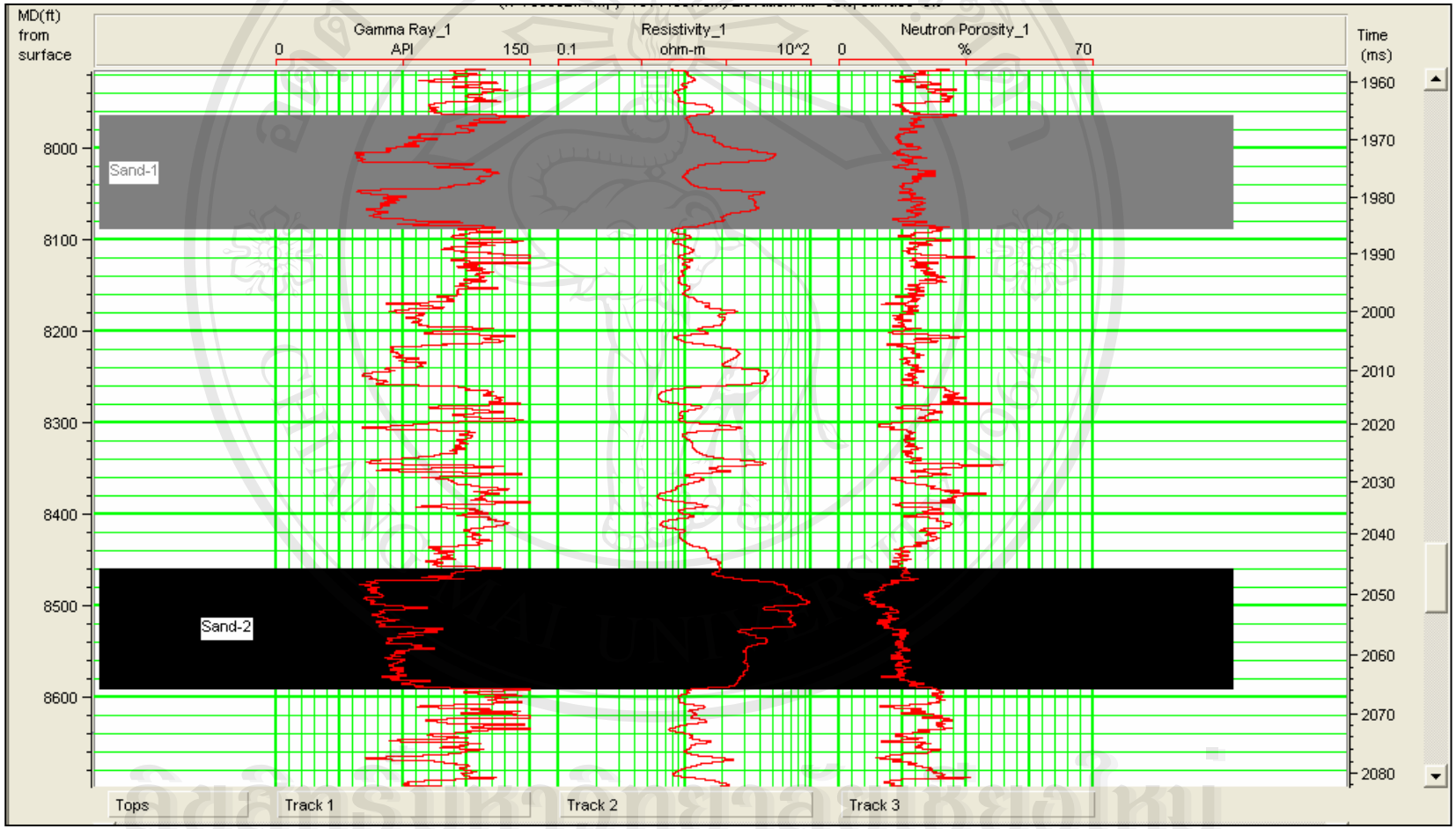

Figure 3.2 Target sandstone layers 1 and 2 in Well-2.

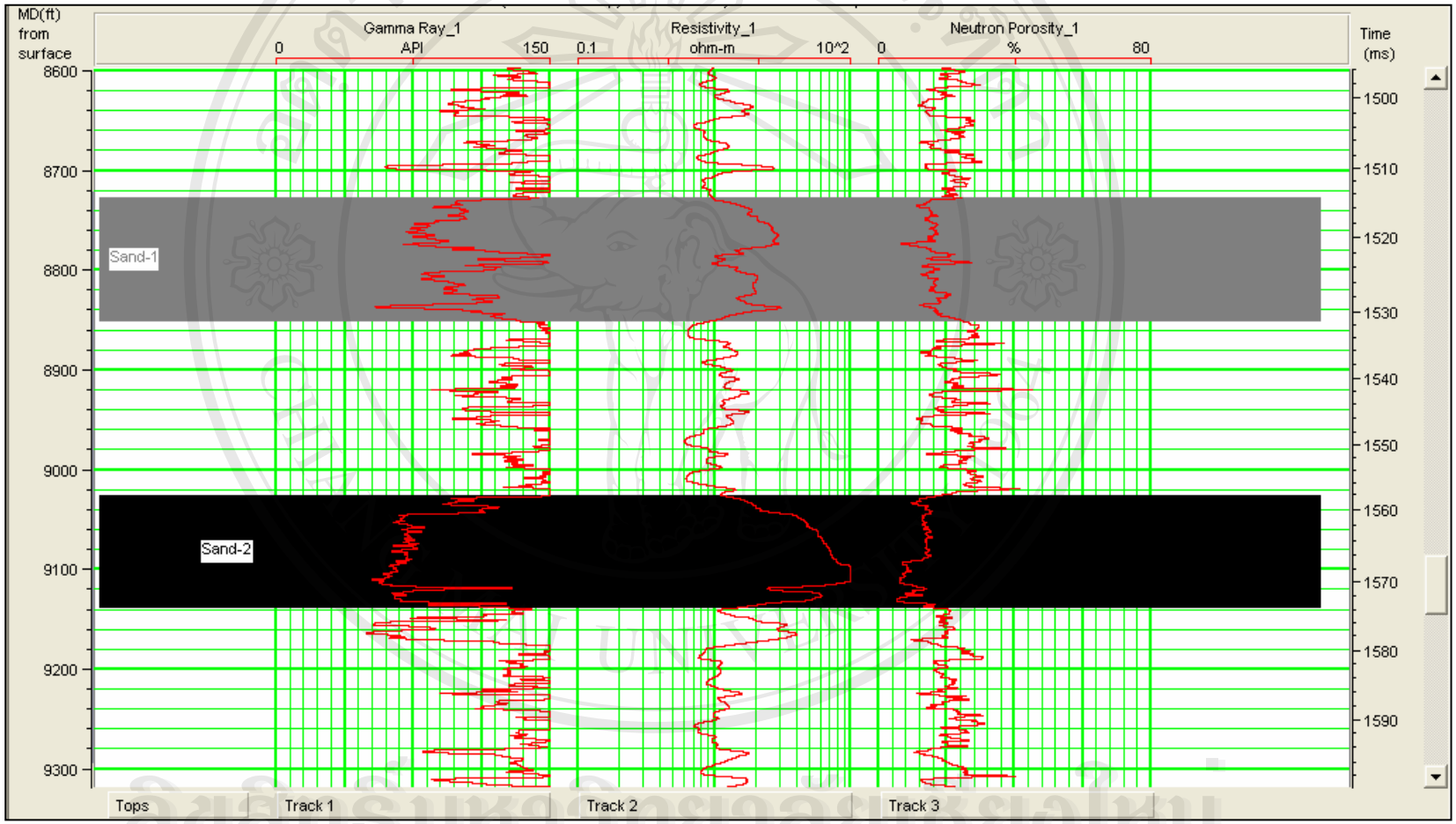

Figure 3.3 Target sandstone layers 1 and 2 in Well-3.

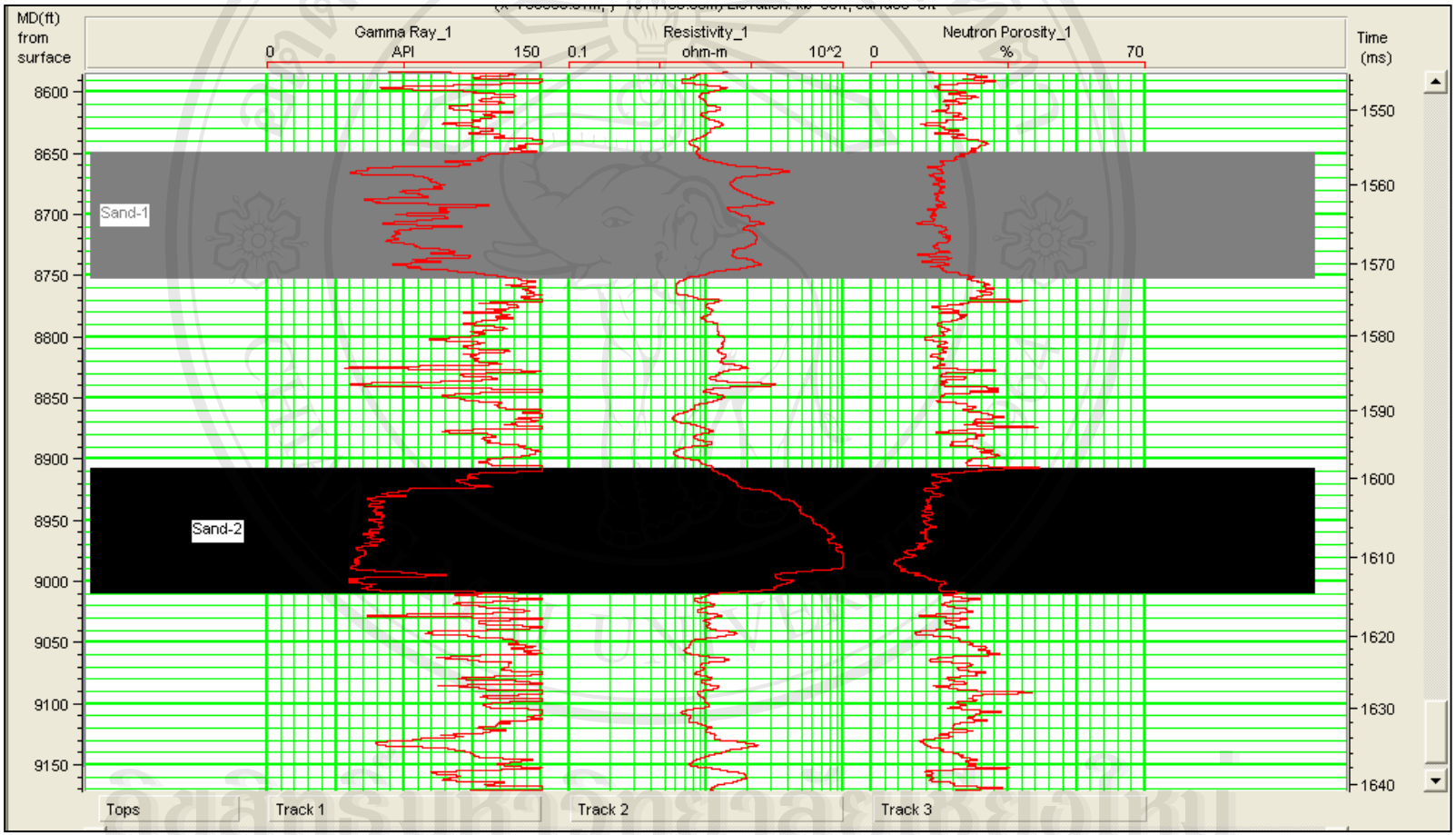

Figure 3.4 Target sandstone layers 1 and 2 in Well-7.

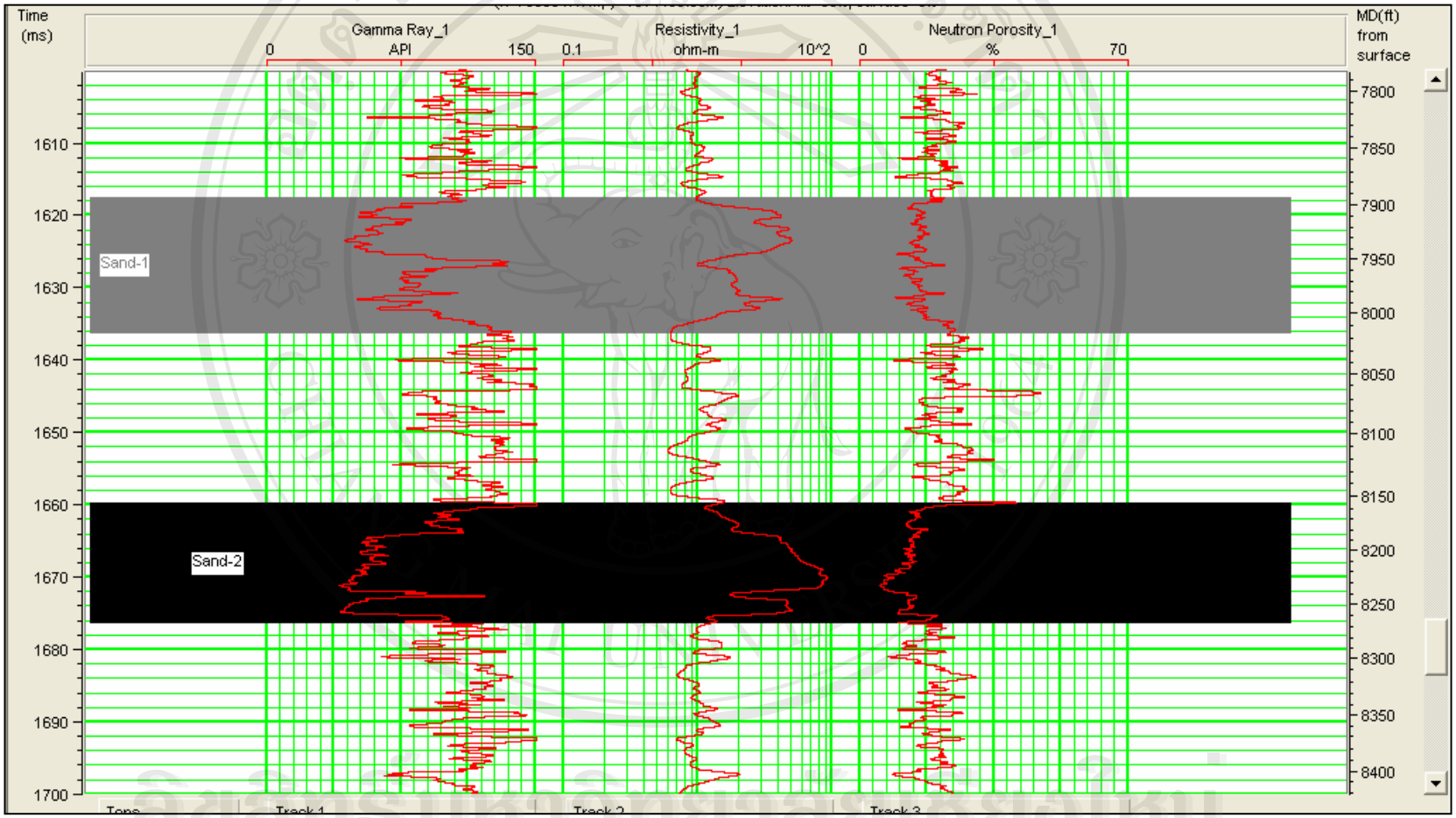

Figure 3.5 Target sandstone layers 1 and 2 in Well-8.

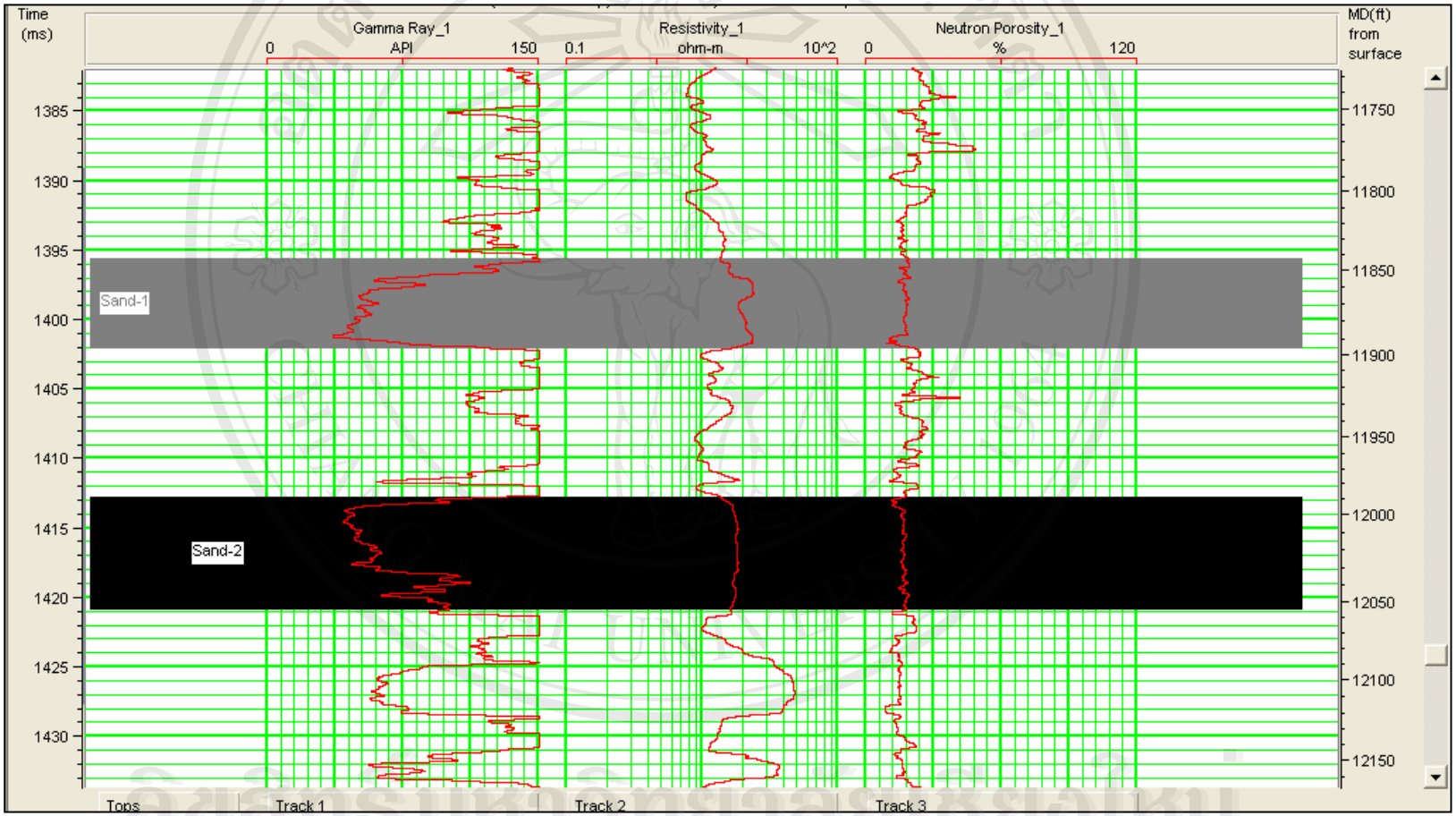

Figure 3.6 Target sandstone layers 1 and 2 in Well-12.

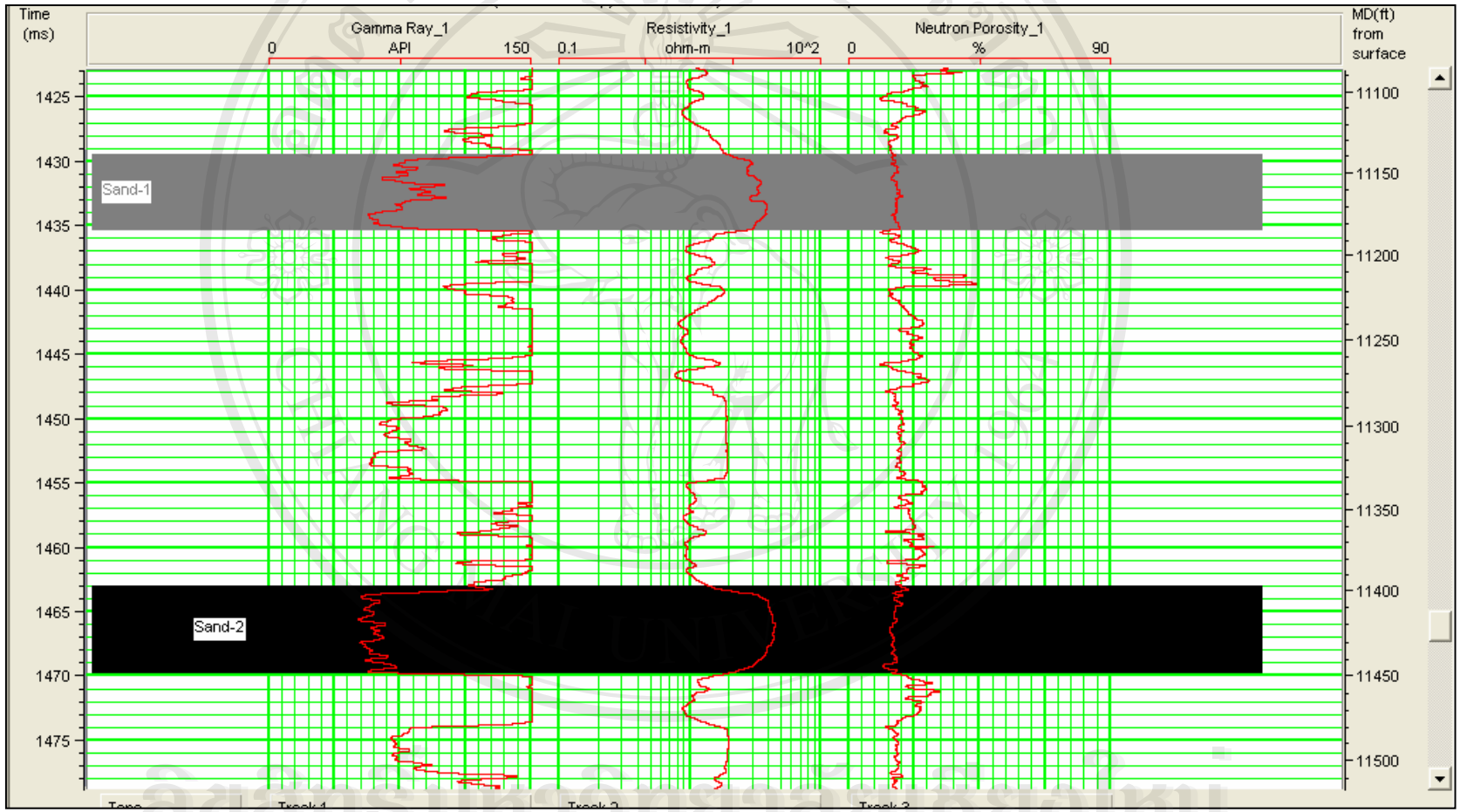

Figure 3.7 Target sandstone layers 1 and 2 in Well-11.

	Well Name	Unit	Sand-1 (top)	Sand-1 (base)	Sand-2 (top)	Sand-2 (base)
1	WELL-1	ft (fr. Surface)	7794.00	7868.00	8090.00	8207.00
2	WELL-2	ft (fr. Surface)	7966.00	8090.00	8461.00	8594.00
3	WELL-3	ft (fr. Surface)	8729.00	8853.00	9027.00	9141.00
4	WELL-7	ft (fr. Surface)	8650.00	8754.00	8909.00	9012.00
5	WELL-8	ft (fr. Surface)	7895.00	8018.00	8157.00	8269.00
6	WELL-11	ft (fr. Surface)	11140.00	11185.00	11398.00	11450.00
7	WELL-12	ft (fr. Surface)	11844.00	11898.00	11990.00	12056.00

Figure 3.8 Summary of the measured depths of sandstones1 and 2 in seven wells.

3.1.2. Wavelet extraction and synthetic generation

Wavelet extraction is an important step in correlating well logs. A better wavelet would be one that is extracted from the seismic data. However, in order to get the correct phase of the wavelet, it is preferable to use sonic well data for wavelet extraction. The Hampson-Russell® eLOG® program has two options for wavelet extraction. These are "Use Well", which uses well log data, and "Statistical**",** which uses seismic data. A statistical wavelet was first extracted from seismic data. This wavelet is a zero-phase wavelet. With this wavelet the correlation field shows a rather low correlation. Next the correlation between synthetic seismogram and seismic data was done by selecting events on the synthetic trace and selecting the corresponding event on the composite trace. After selecting the events, stretching was performed on the well logs. The process of correlation is exactly similar to applying a manual check-shot correction.

With a correlated log, a better wavelet was extracted using the well logs to determine the phase of the wavelet. First, only the current well was used to extract a new wavelet. This extracted wavelet appears to include noise. It was improved by using data from all wells in wavelet extraction. The final resulting wavelet was better and the general correlation was improved. When this final wavelet (Figure 3.9) was used, a multi-well analysis had a total correlation of 0.30 (Figure 3.15). This plot was used to evaluate how well the extracted wavelet fitted each of the seven wells. This wavelet extraction procedure was done on each well. This resulted in an average, and better, wavelet to use for correlation purpose (Figure 3.9). Figures 3.10 to 3.14 show the synthetic seismograms correlated to five wells that have better correlation. These

five wells were used to generate acoustic impedance volume and to analyze attributes for porosity prediction.

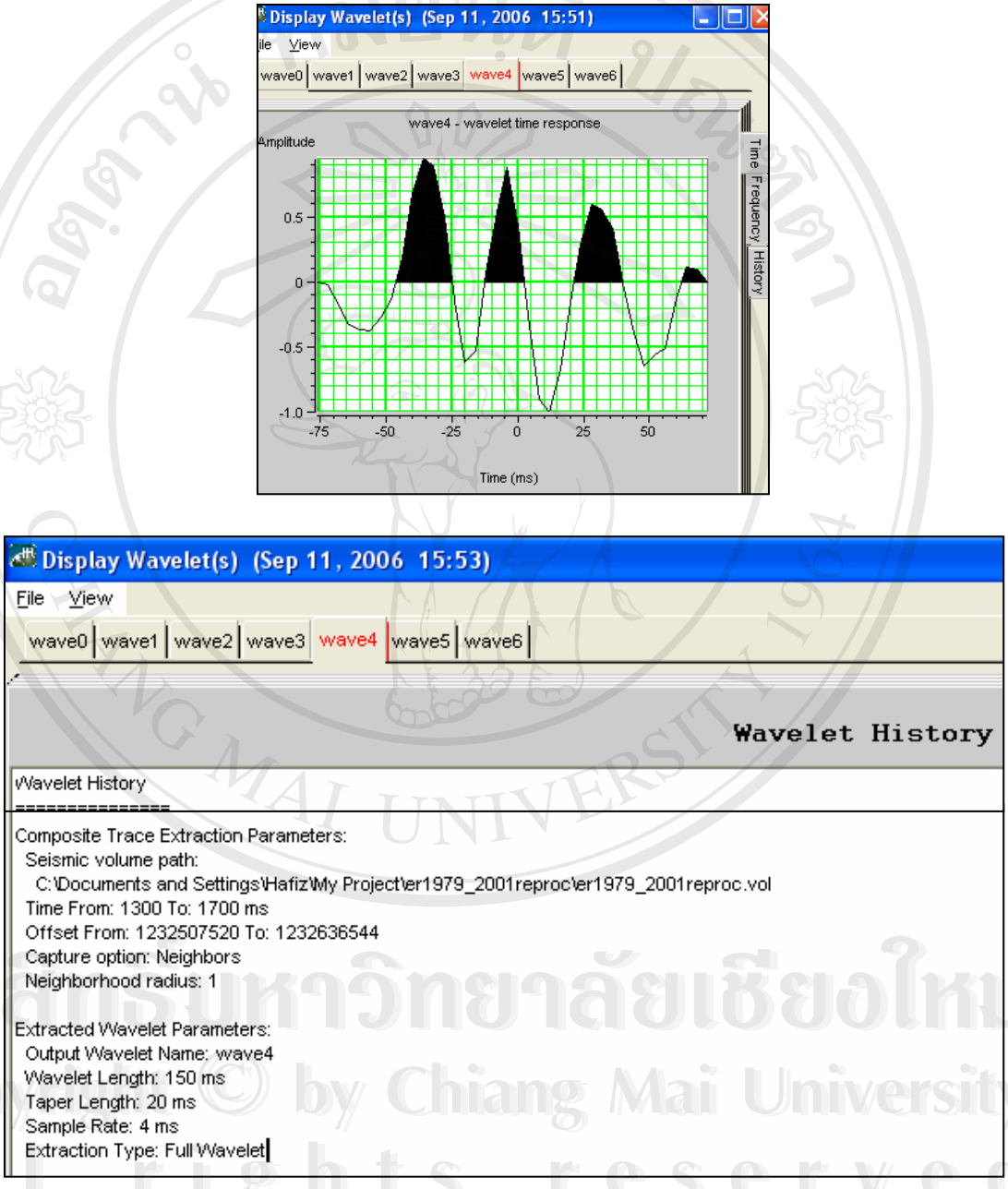

Figure 3.9 The final wavelet and its generation history

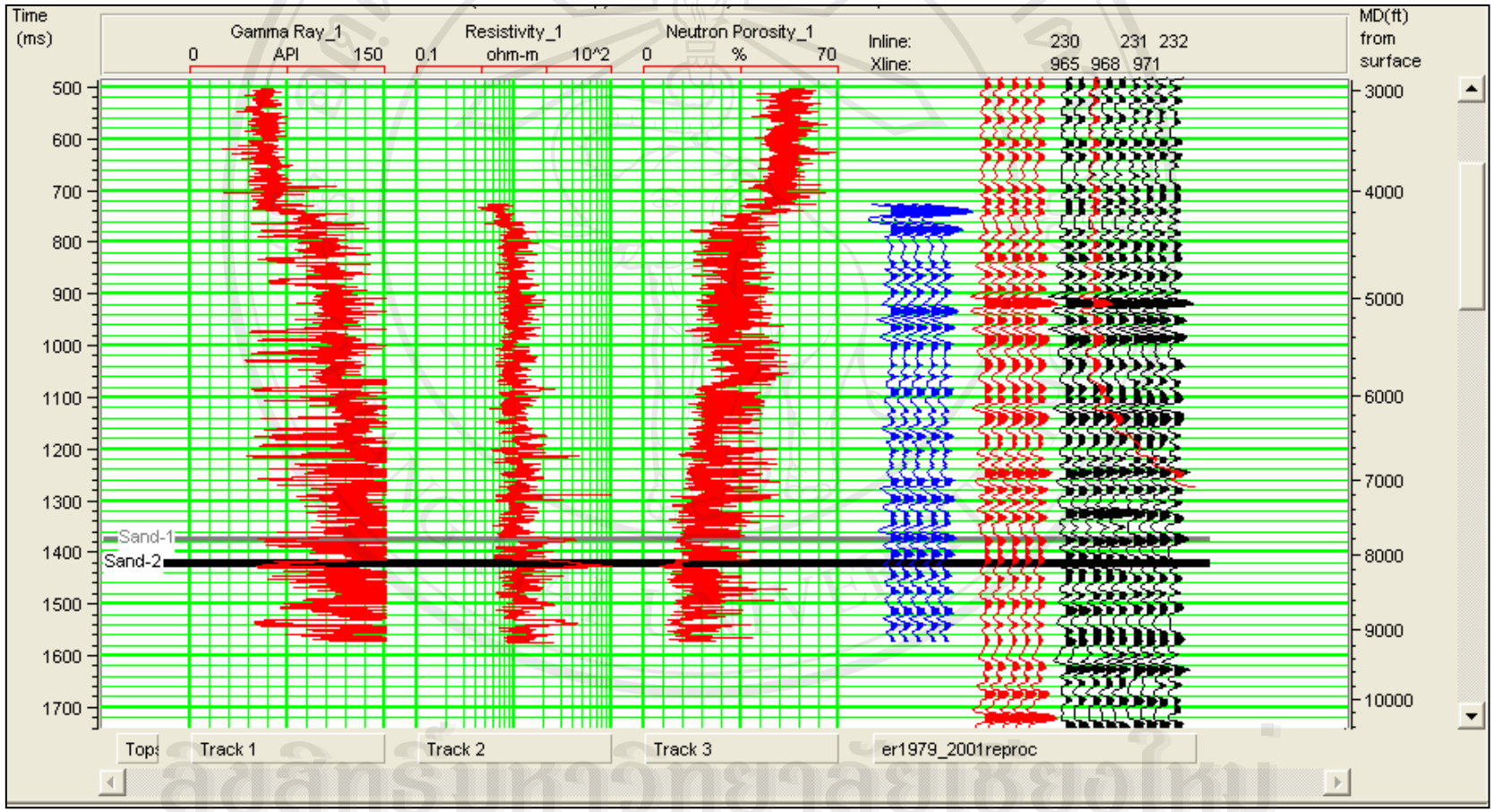

Figure 3.10 Synthetic seismogram of Well-1.

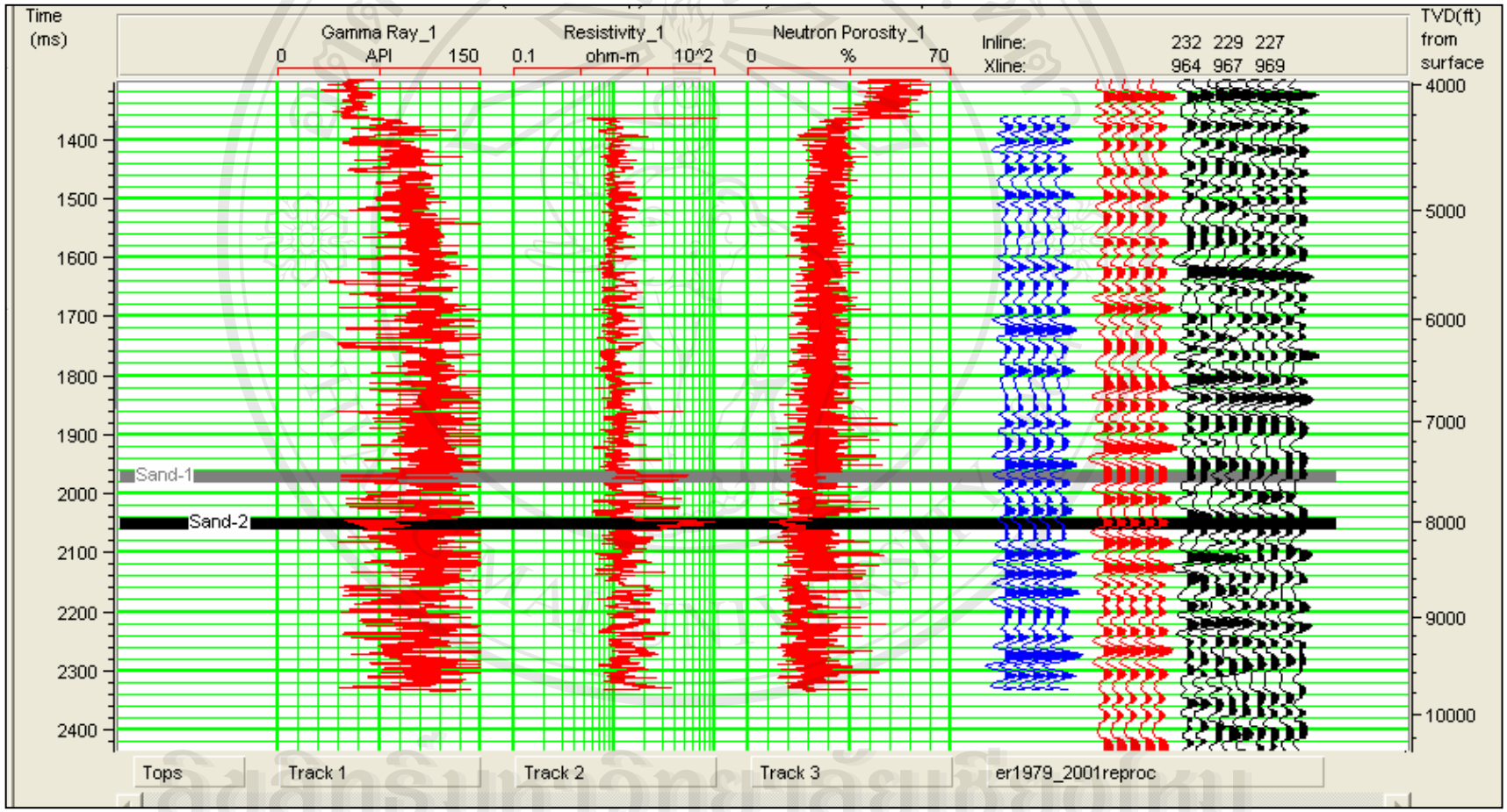

Figure 3.11 Synthetic seismogram of Well-2.

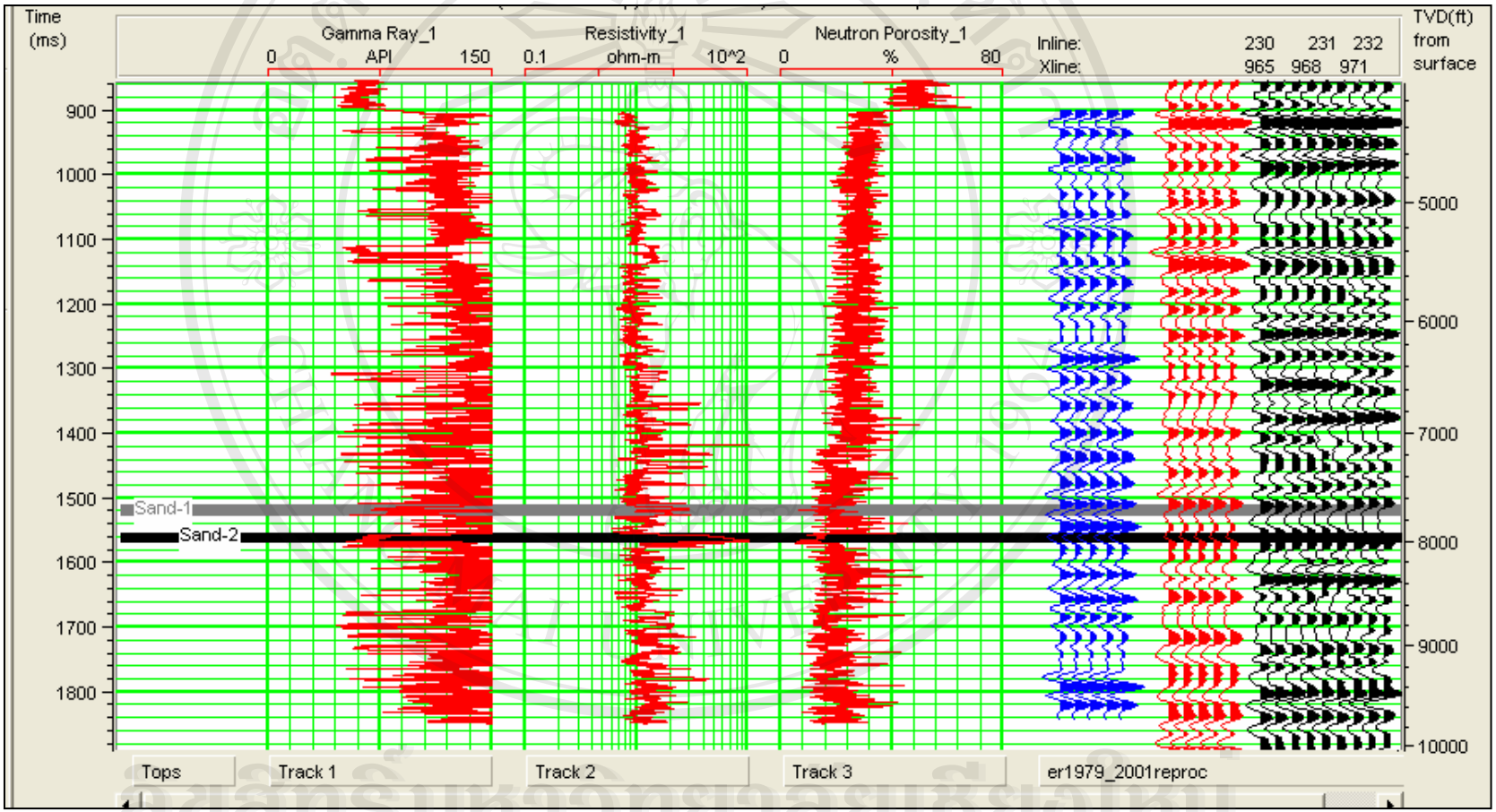

Figure 3.12 Synthetic seismogram of Well-3.

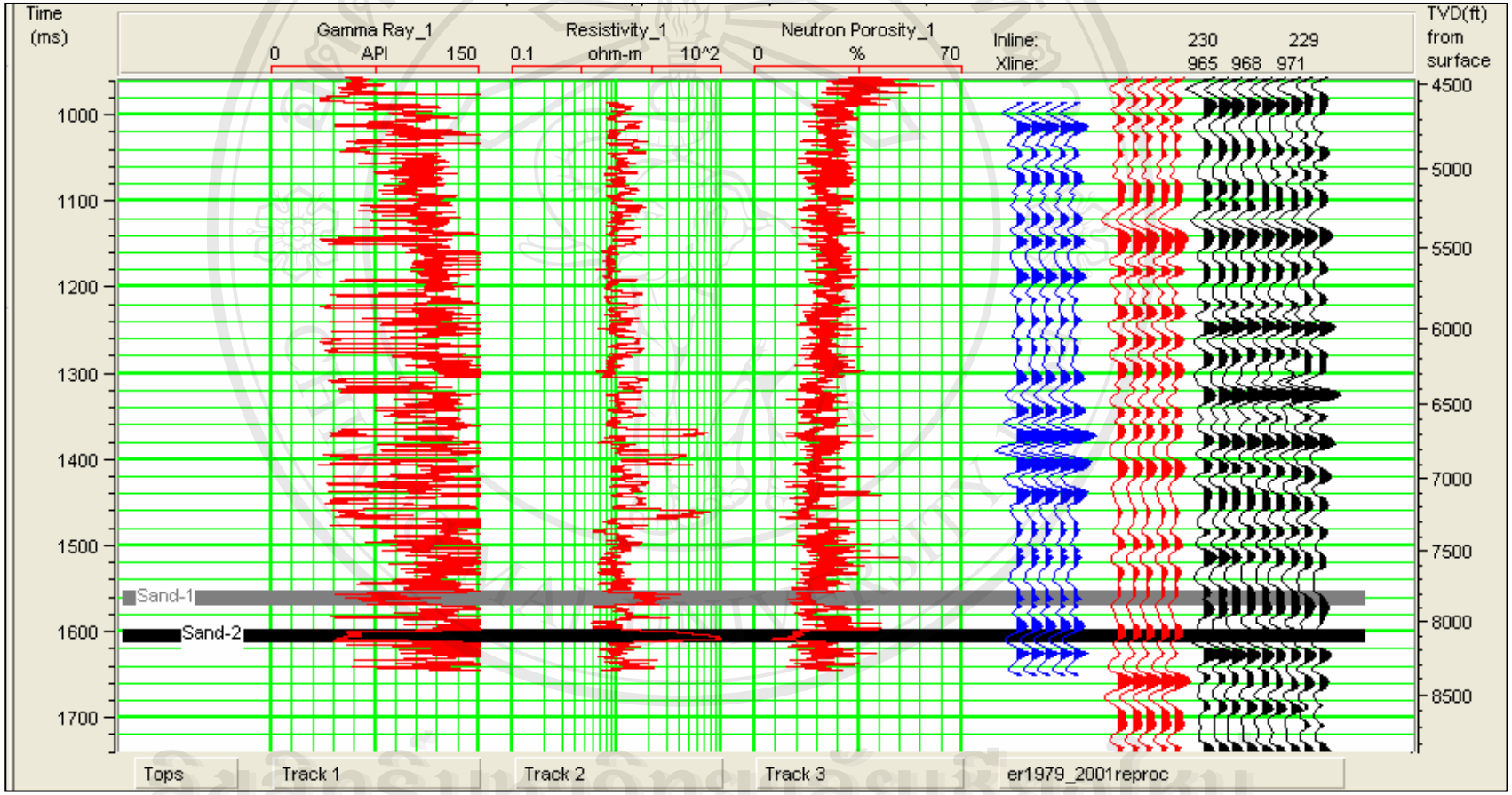

Figure 3.13 Synthetic seismogram of Well-7.

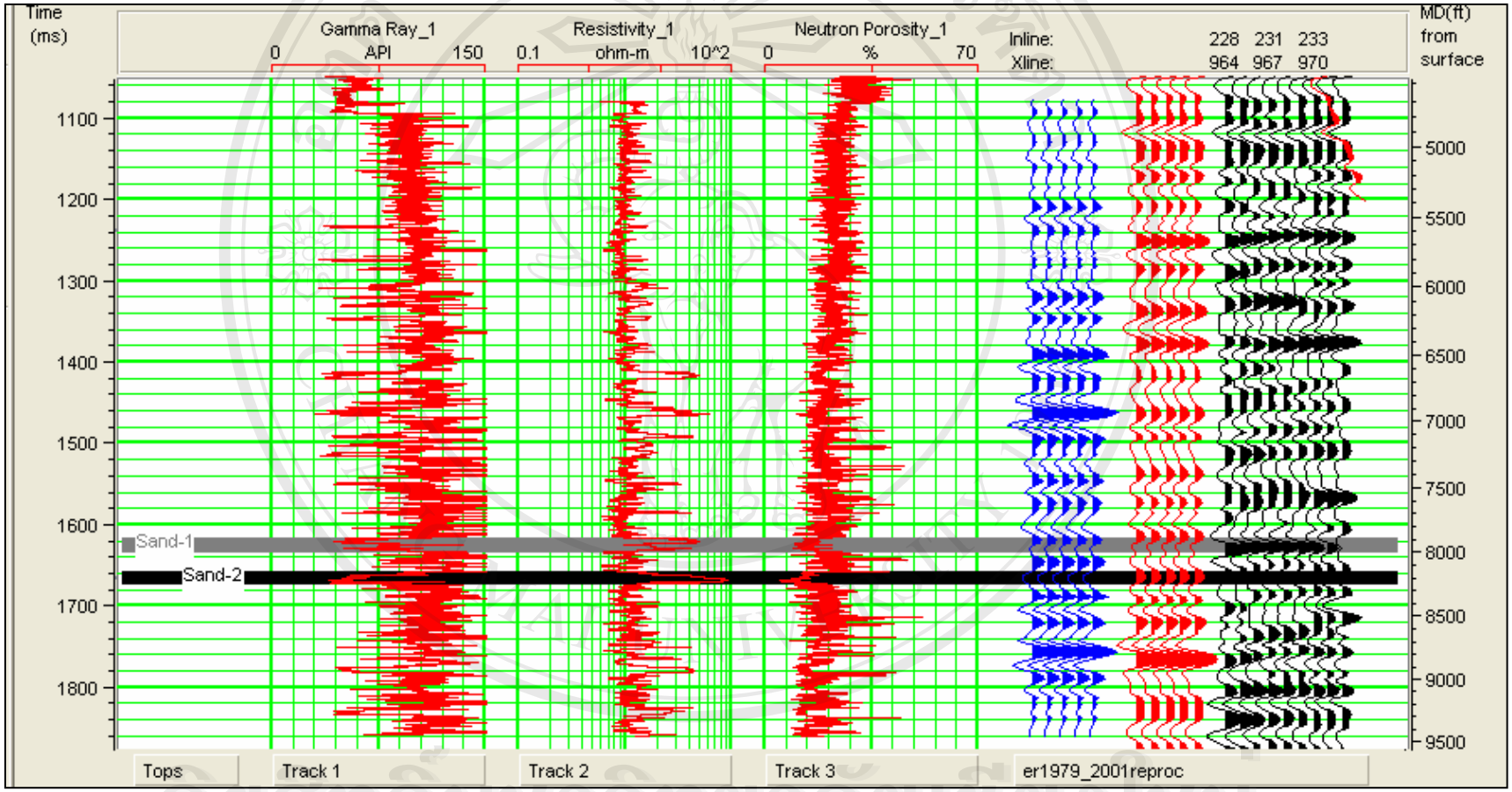

Figure 3.14 Synthetic seismogram of Well-8.

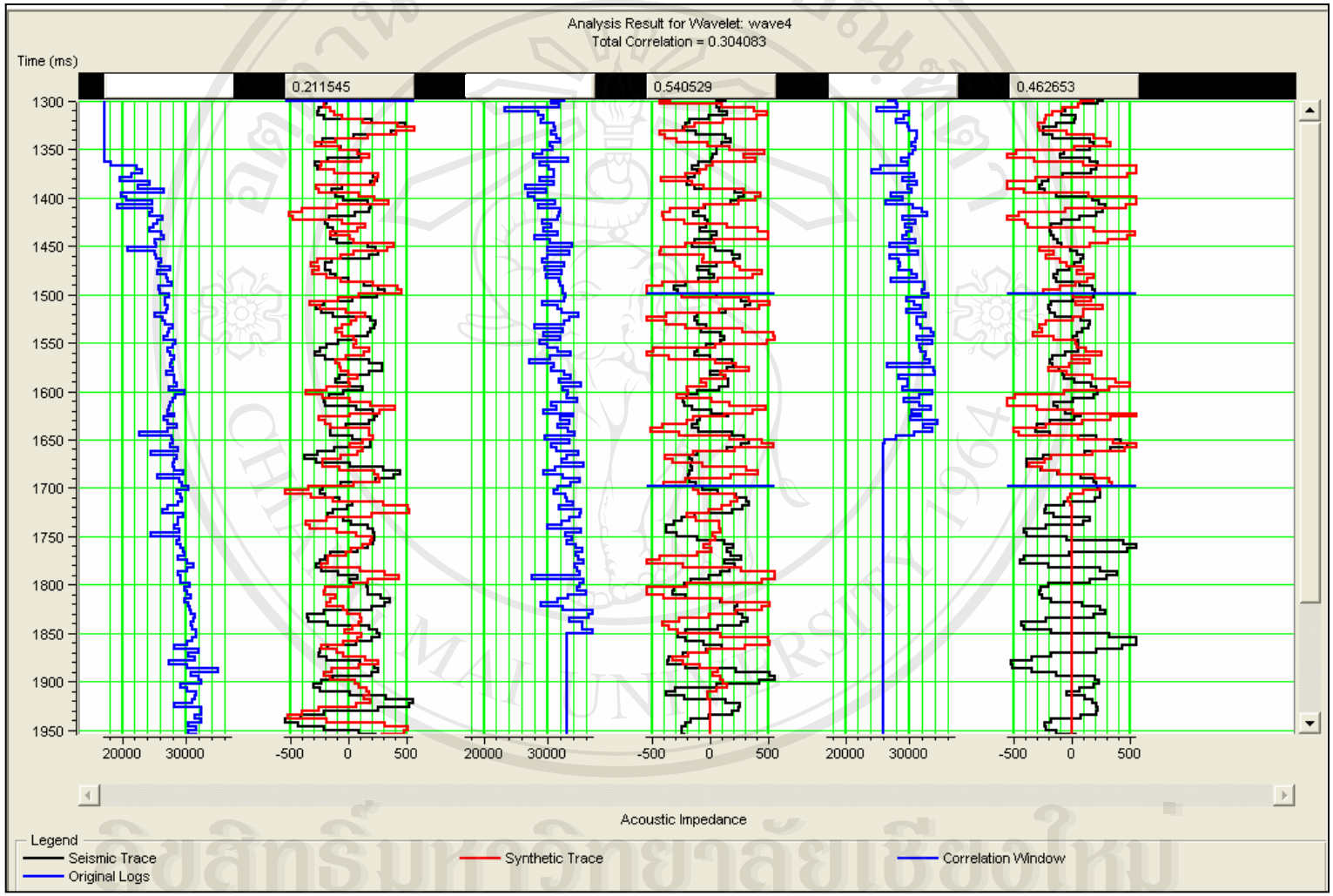

Figure 3.15 Multi-well analysis showing a total correlation of 0.30.

3.2 Generation of acoustic impedance volume

The STRATA® program was used to generate an acoustic impedance inversion volume for use in the EMERGE® program as an external attribute. The STRATA® program has several inversion methods and its model-based inversion method was used in this study. Since all inversion algorithms suffer non-uniqueness, it is important to use some external information to limit the number of possible models that can agree with the input seismic data. Well log data provide the additional information needed to constrain the model and to make the inversion result more accurate.

An initial background model was formed by picking three continuous horizons in the input seismic volume (Figure 3.16). Before that, well correlation and wavelet extraction was carried out in the eLOG® program. The model-based inversion method was then applied to generate an acoustic impedance volume. The inversion parameters chosen were:

- Inversion option - constrained
- Average block size – 8 milliseconds
- Number of iterations – 10
- Processing sample rate – 4 milliseconds
- Separate scaler for each trace
- Single trace inversion

Figures 3.17 and 3.18 show that impedance increases with depth. The color bar on the right in the figures gives a total impedance range for the particular section. Since the impedance is a product of density and velocity, it is measured in feet per second x grams per cubic centimeter.

The STRATA® program gives a model-based derived synthetic error plot (Figure 3.19) as a check of the inversion result. This check is the difference between the original seismic data and the synthetic calculated from the inversion result. For this study, it is close to zero and indicates successful inversion.

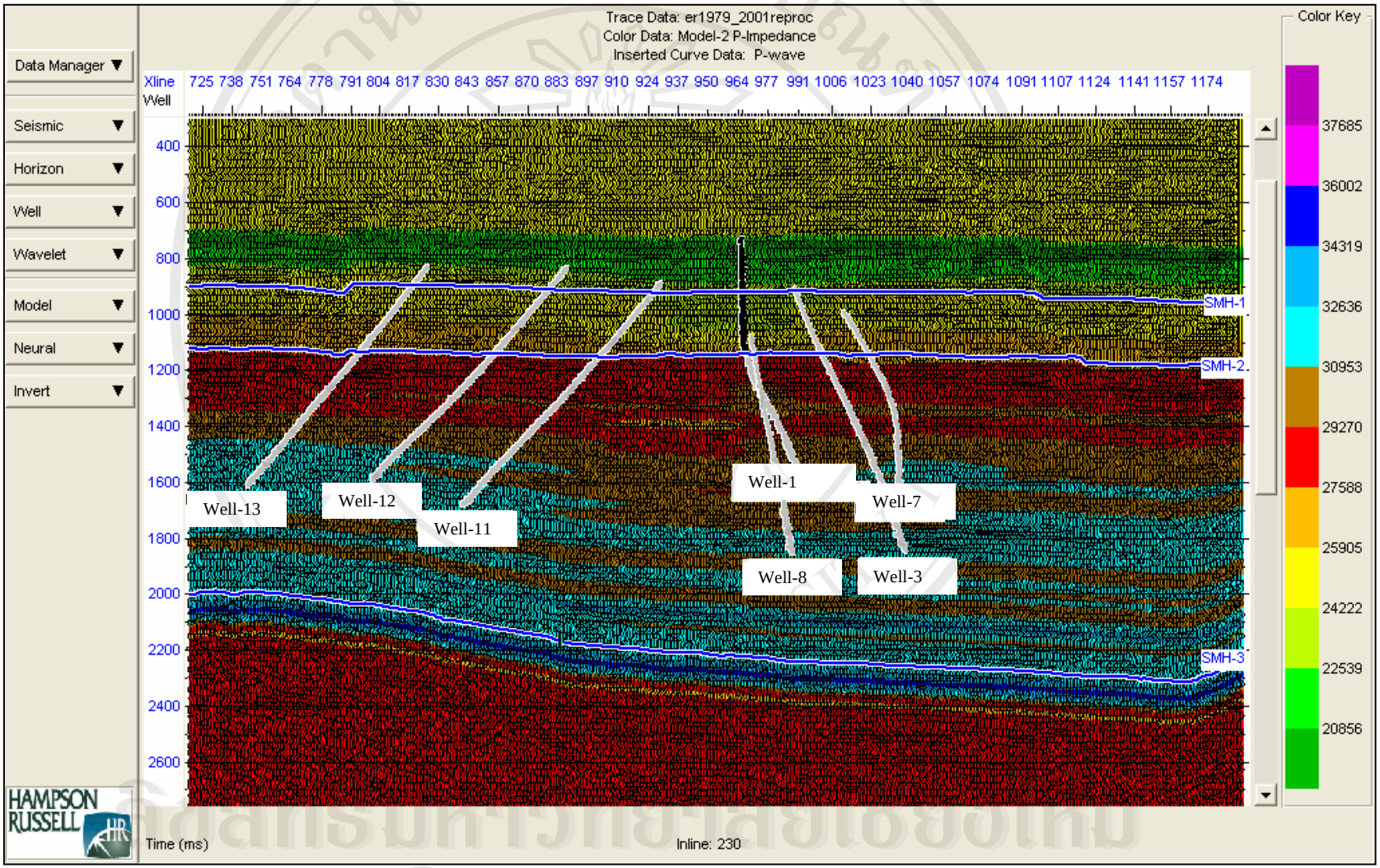

Figure 3.16 Initial background model.

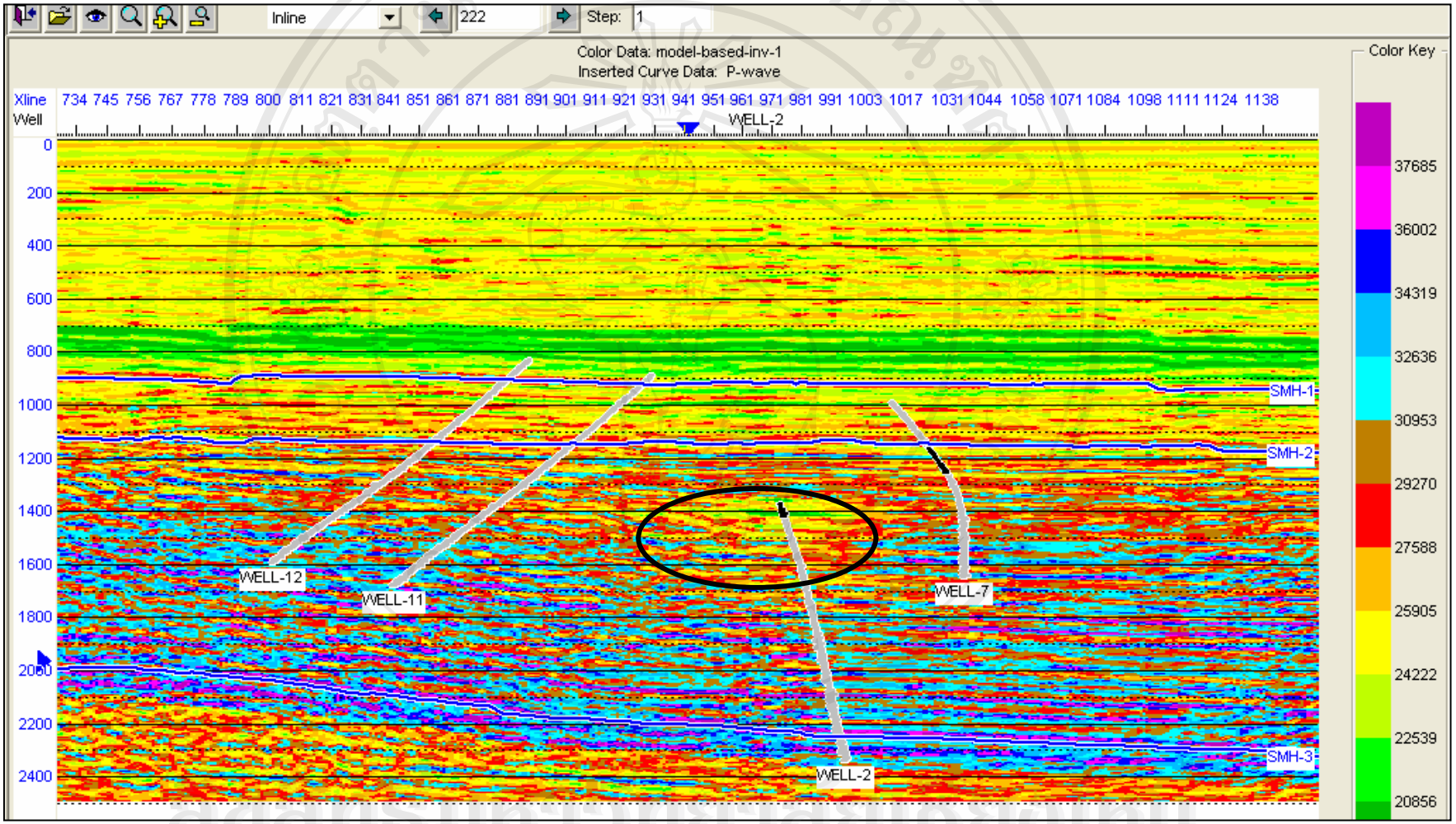

Figure 3.17 Model-based inversion result-acoustic impedance section inline 222. (inversion is applicable between SMH-1 and SMH-3).

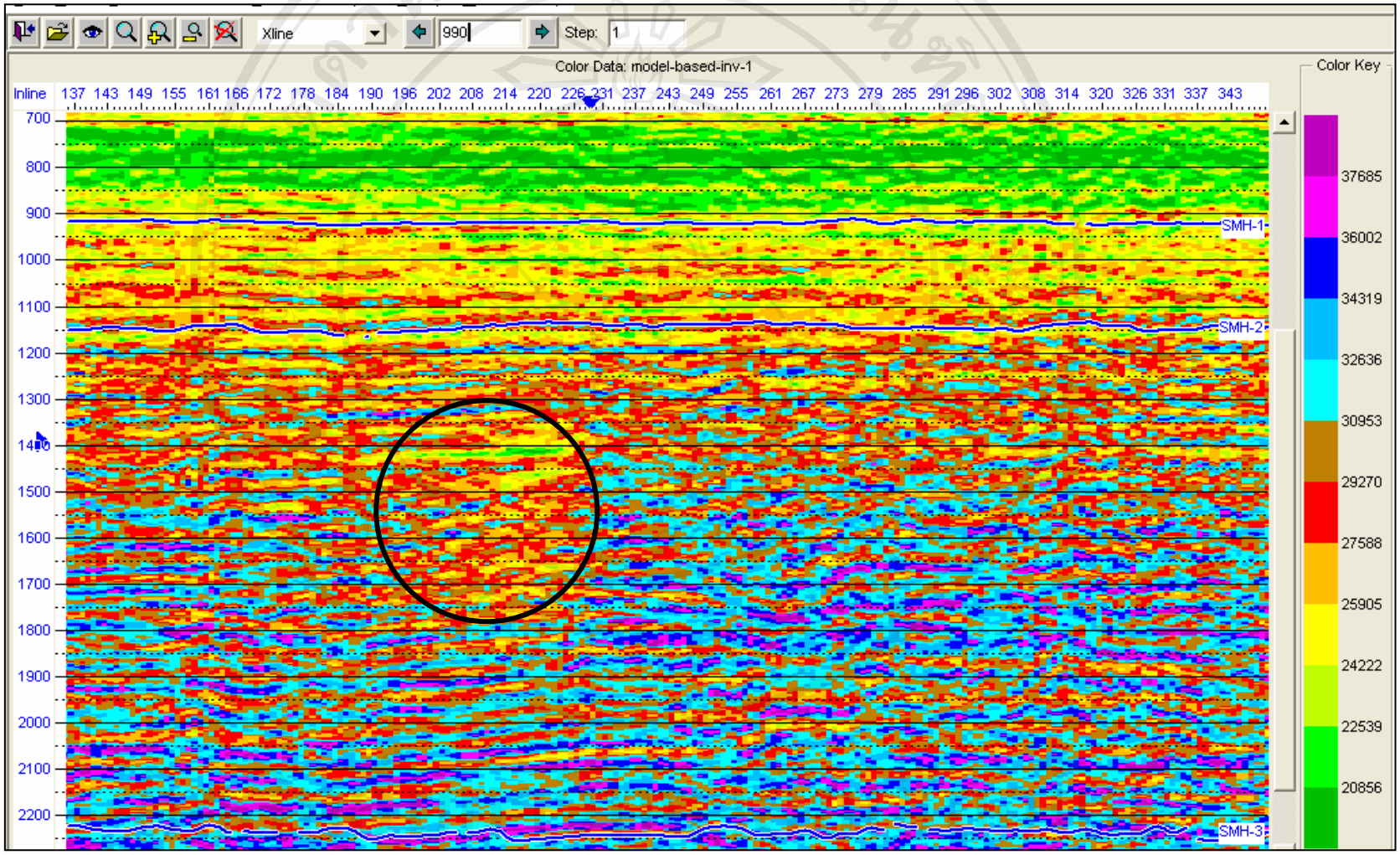

Figure 3.18 Model-based inversion result-acoustic impedance section crossline 990 (inversion applicable between SMH-1 and SMH-3).

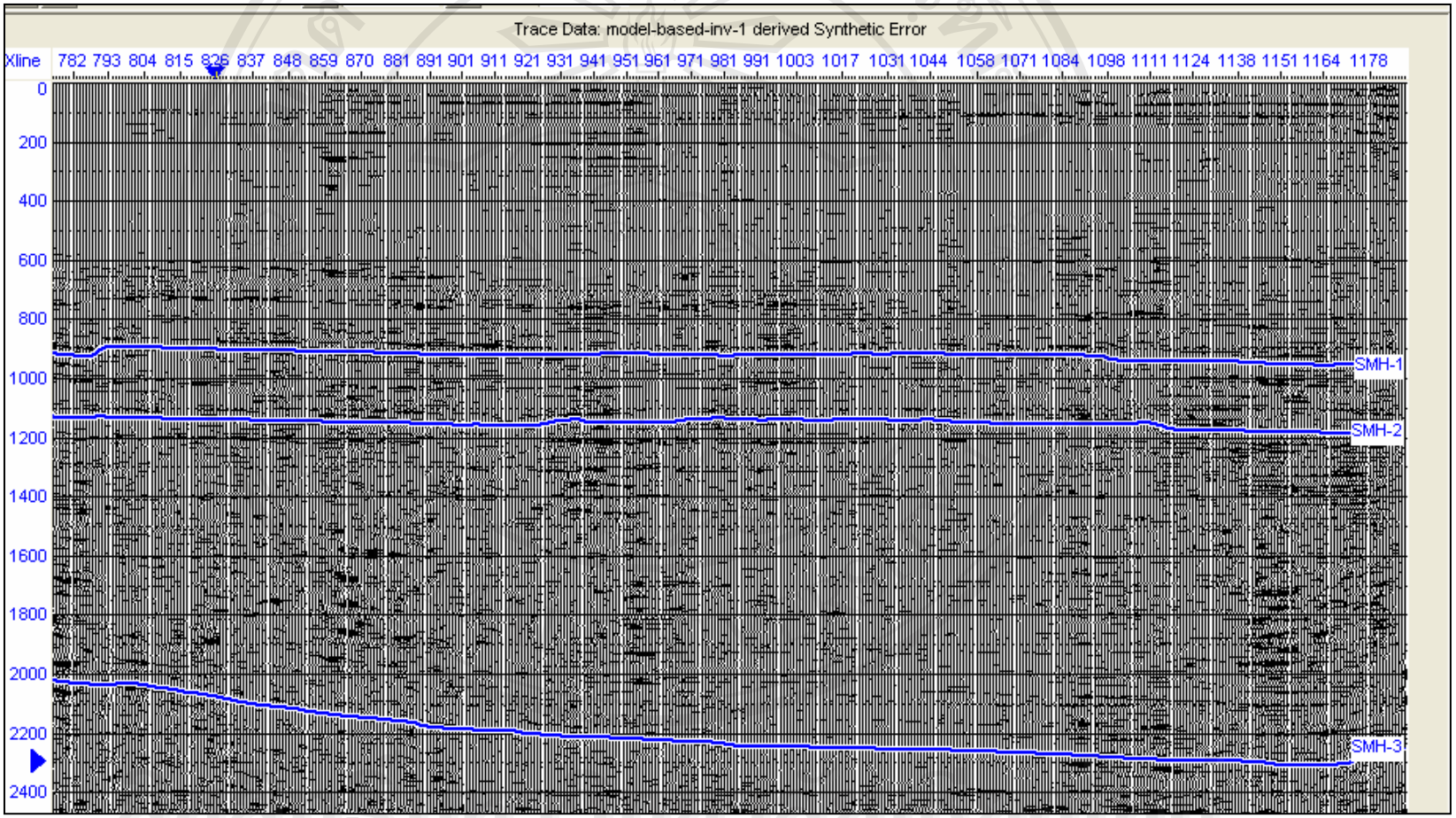

Figure 3.19 Model-based inversion derived synthetic error.

3.3 Attribute analysis and porosity prediction

3.3.1 Density-porosity logs

Porosity is one of the important reservoir properties because it determines the volume of fluids in a reservoir. The Hampson-Russell® eLOG® program calculates density porosity and was used to calculate the density porosity for each of the seven wells. The program used the standard density-porosity formula (Figure 3.20), using fluid density of seawater and matrix density of quartz sandstone. The program default values for matrix density and fluid density has been used in the study due to the confidentiality of such data. The use of real field data in this might change the absolute values of porosity in the final prediction steps. The resulting density-porosity logs were used as target porosity logs for attribute analysis in the EMERGE® program.

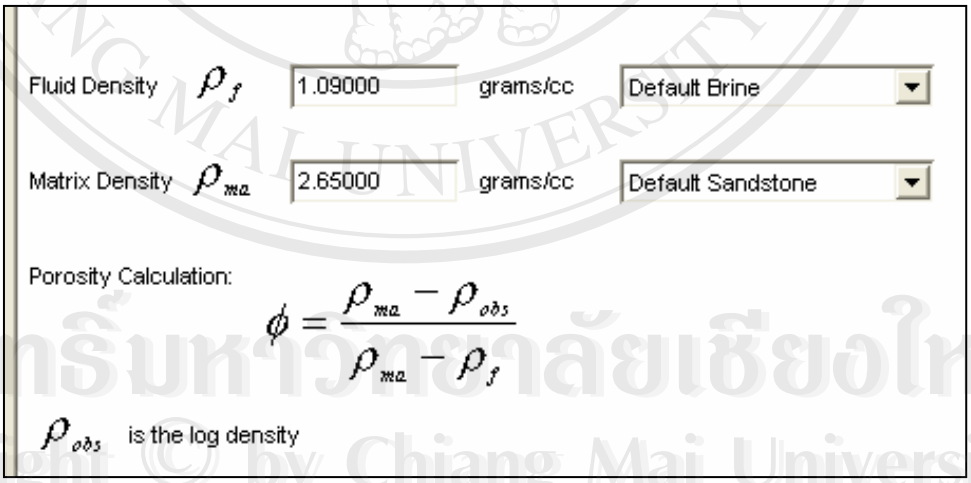

Figure 3.20 Formula and constants used to calculate porosity from density logs.

3.3.2 Attribute analysis

The multi-regression analysis method was used for attribute analysis. Figure 3.21 shows the input data for attribute analysis: target porosity log in red, the single seismic trace in black, and the acoustic impedance as an external attribute in blue. Brown horizontal bars indicate the analysis window, which may be different from well to well.

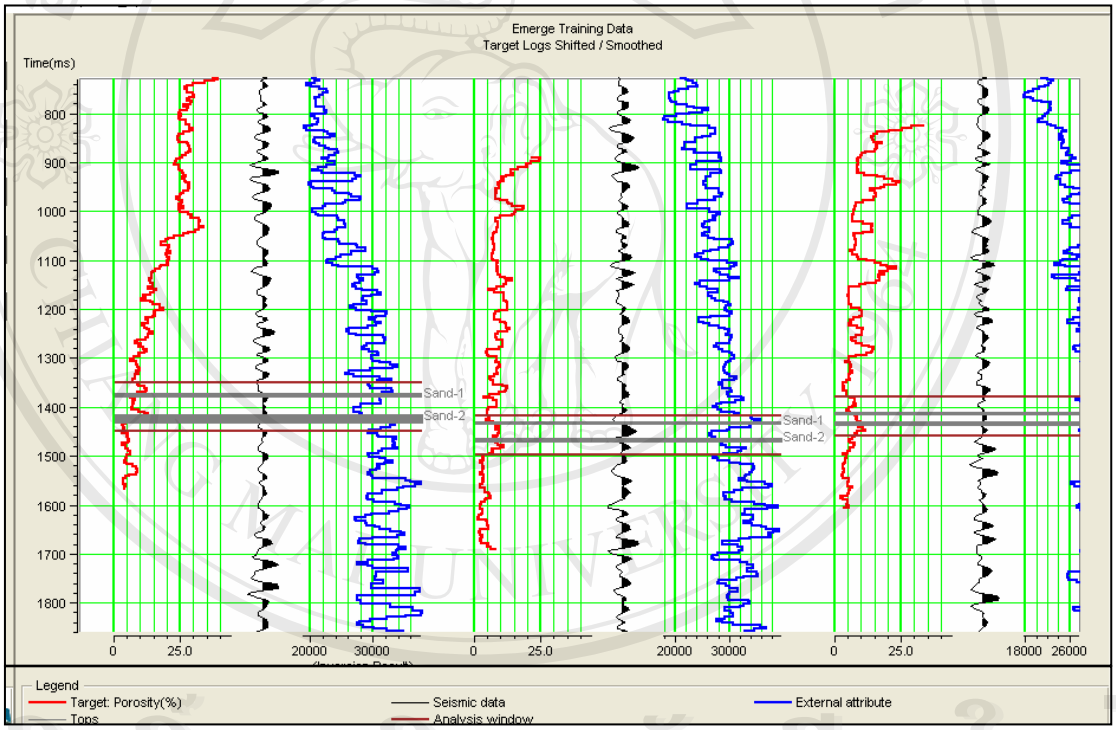

Figure 3.21 Input data to the EMERGE® program for performing attribute analysis.

Multi-attribute regression was done using seven attributes as the maximum number. Figure 3.22 is the multi-attribute table and it shows the result of the calculation. Each row in the table corresponds to a particular multi-attribute transform and includes all the attributes above it. For example, the first row, labeled inversion

result, indicates that the single best attribute to use alone is the inversion result. The second row, apparent polarity, refers to a transform using both the inversion result and the apparent polarity simultaneously. This is the best pair. The other rows, in succession, are the best triplet to the best seven. The decreasing error shows that, as expected, the prediction error decreases with increasing number of attributes.

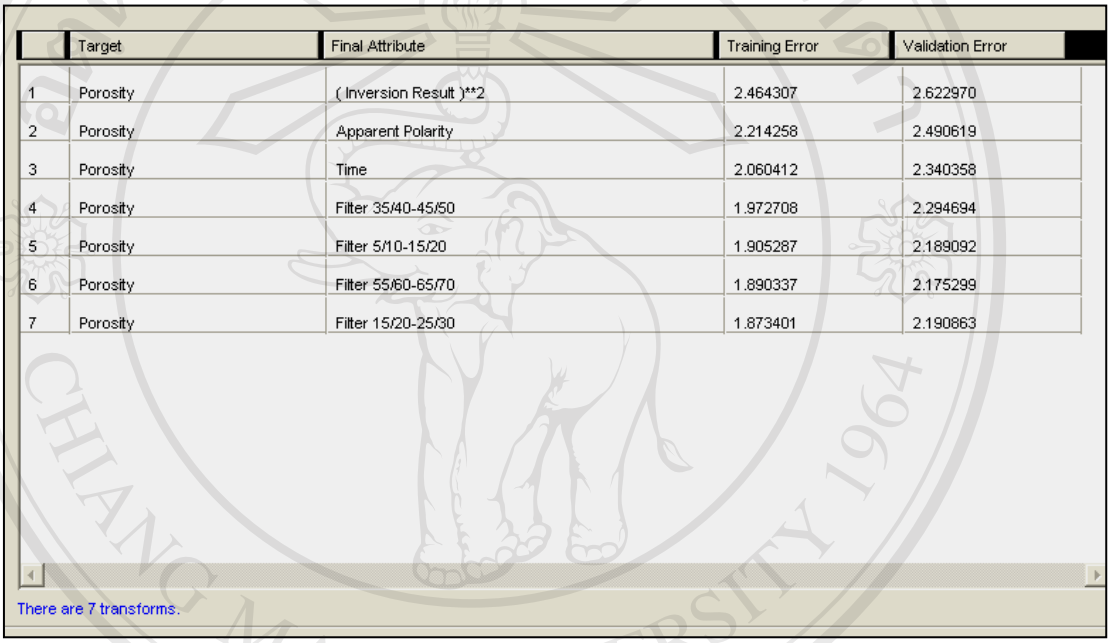

	Target	Final Attribute	Training Error	Validation Error
1	Porosity	(Inversion Result)**2	2.464307	2.622970
2	Porosity	Apparent Polarity	2.214258	2.490619
3	Porosity	Time	2.060412	2.340358
4	Porosity	Filter 35/40-45/50	1.972708	2.294694
5	Porosity	Filter 5/10-15/20	1.905287	2.189092
6	Porosity	Filter 55/60-65/70	1.890337	2.175299
7	Porosity	Filter 15/20-25/30	1.873401	2.190863

There are 7 transforms.

Figure 3.22 Multi-attribute regression results.

Figure 3.23 is the graphical representation of the multi-attribute table of Figure 3.22. The black curve of the figure shows the prediction error on the vertical axis and the number of attributes on the horizontal axis. Mathematically, this curve should always decrease. It should always be true that adding more attributes will predict data better. This does not always mean that the added attributes are predicting the true signal in the target log. Eventually, adding more attributes will simply predict the details, or noise, in the log or in the attributes themselves. The red curve is the validation error. This error is used to decide when too many attributes have been

added. Each point in the validation error was calculated by hiding each well and predicting its values using the operator calculated from the other wells. For example, the last red point, corresponding to seven attributes, was calculated as follows: the seven attribute types were arranged according to the table in Figure 3.22. First, well 1 was removed from the calculation. The weights for the seven attributes were calculated using the other four wells in the analysis. The derived operator was then used to predict the values at well 1. Since the exact values for well 1 are already known, the root mean square error for well 1 was stored. This process was repeated for the other wells. The last point on the validation curve is the average error for all of the wells calculated this way. It represents the expected error if a new well was predicted. For this reason, the validation curve is a good measure of the validity of the analysis. The validation curve in Figure 3.23 shows that the maximum number of attributes to use is six since there is no improvement in the validation error when a seventh attribute is used.

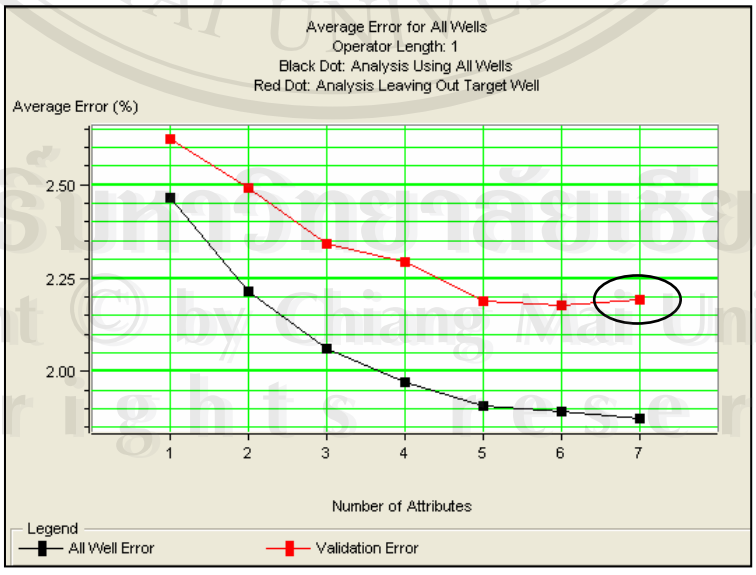

Figure 3.23 Average error as a function of the number of attributes.

Figure 3.24 is the cross plot between the predicted porosity and the actual porosity. It shows that the use of six attributes results in a cross correlation of 74 percent, with an average error of 1.89. The red line is not a regression line but a line with zero intercept and slope of 1, indicating perfect correlation.

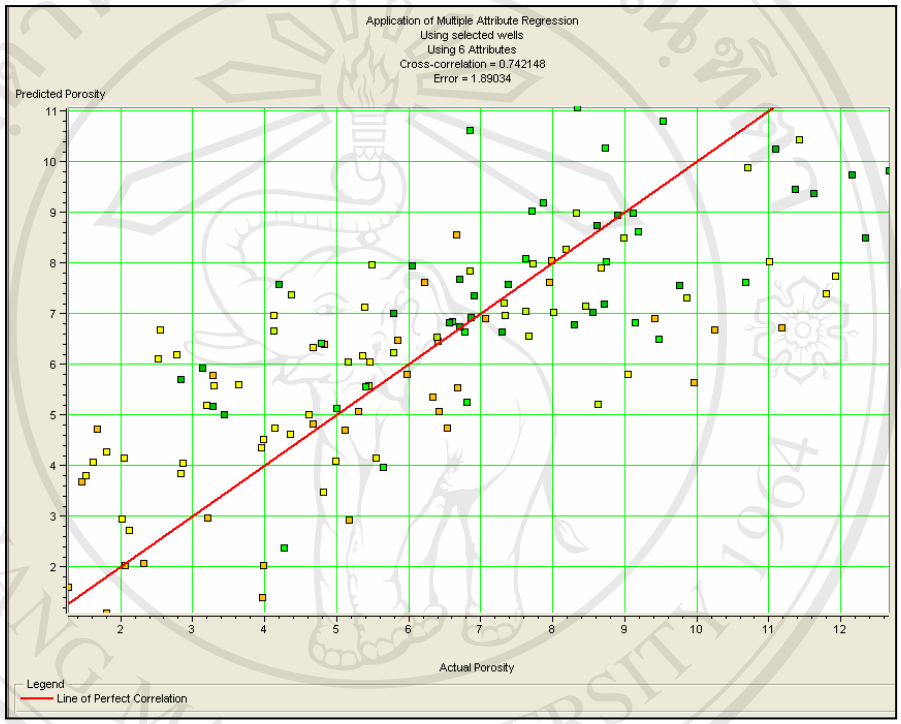

Figure 3.24 Cross plot between predicted porosity and actual porosity.

Figure 3.25 shows that when the derived relationship was used to predict a porosity log, correlation between the predicted log and the actual log is 74 percent. Figure 3.26 shows that the validation of the predicted log gives 65 percent correlation.

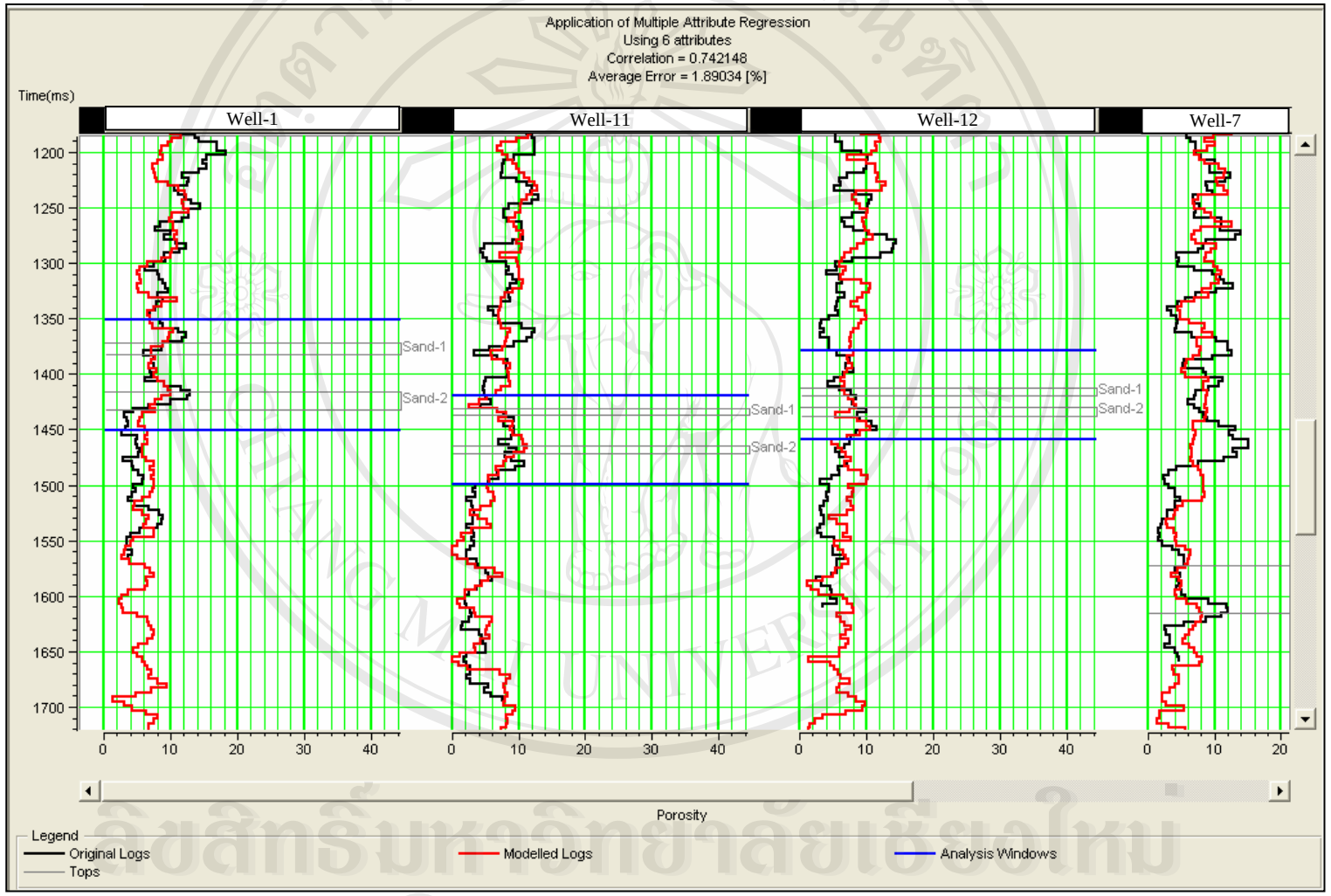

Figure 3.25 Plot of predicted and actual porosity logs applying prediction error.

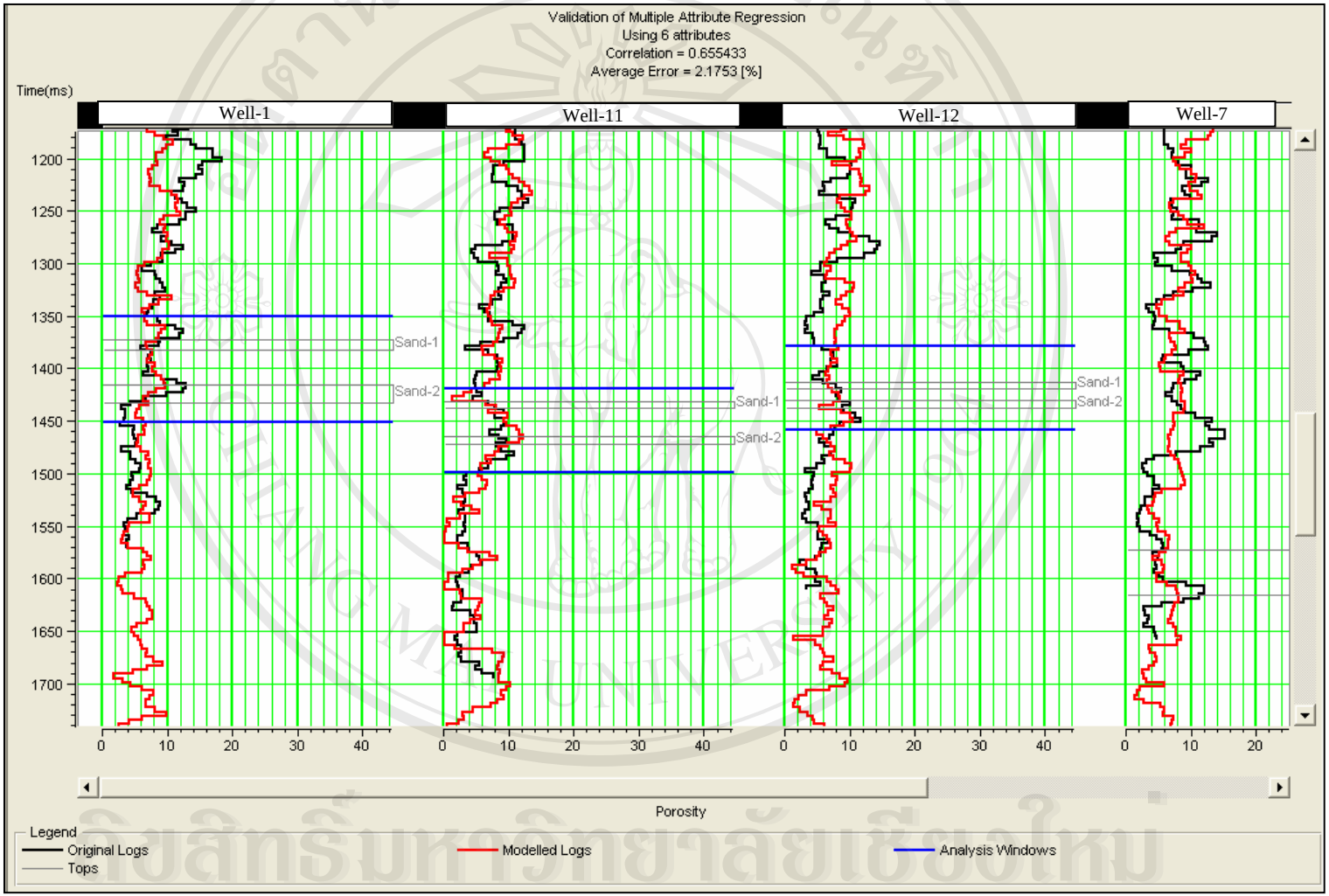

Figure 3.26 Plot of predicted and actual porosity logs applying validation error.

After the relationship between the seismic attributes and porosity logs was determined, it was applied to the seismic data volume. This application was restricted to a time range between 1000 to 2100 milliseconds. The zone of interest is within this time range. Figure 3.27 is an inline section from the predicted porosity volume and Figure 3.28 is a crossline section. A number of time slices were made to show the porosity distribution at different levels in the study area.

3.4 Interpretation

Predicted porosity sections and time slices at different levels were interpreted to find geological features of interest. Figures 3.27 and 3.28 are examples of porosity sections that show some interesting porosity anomalies. The circled zones in the figures are relatively higher porosity patches at the level of relatively low porosity. These anomalies may be interpreted as higher porosity channel sandstone beds. These channel sandstone bodies are probably surrounded by lower porosity flood plain mudstone, represented by yellowish patches in the porosity sections. The other possible interpretation of these porosity anomalies is that they are attributed to fault related lithology variations.

The target sandstone layers 1 and 2 have a correlation at about 1400 milliseconds in the seismic sections along the well-1. Figure 3.29 shows a time slice at a constant time 1400 milliseconds through the porosity volume. This is a type of porosity map.

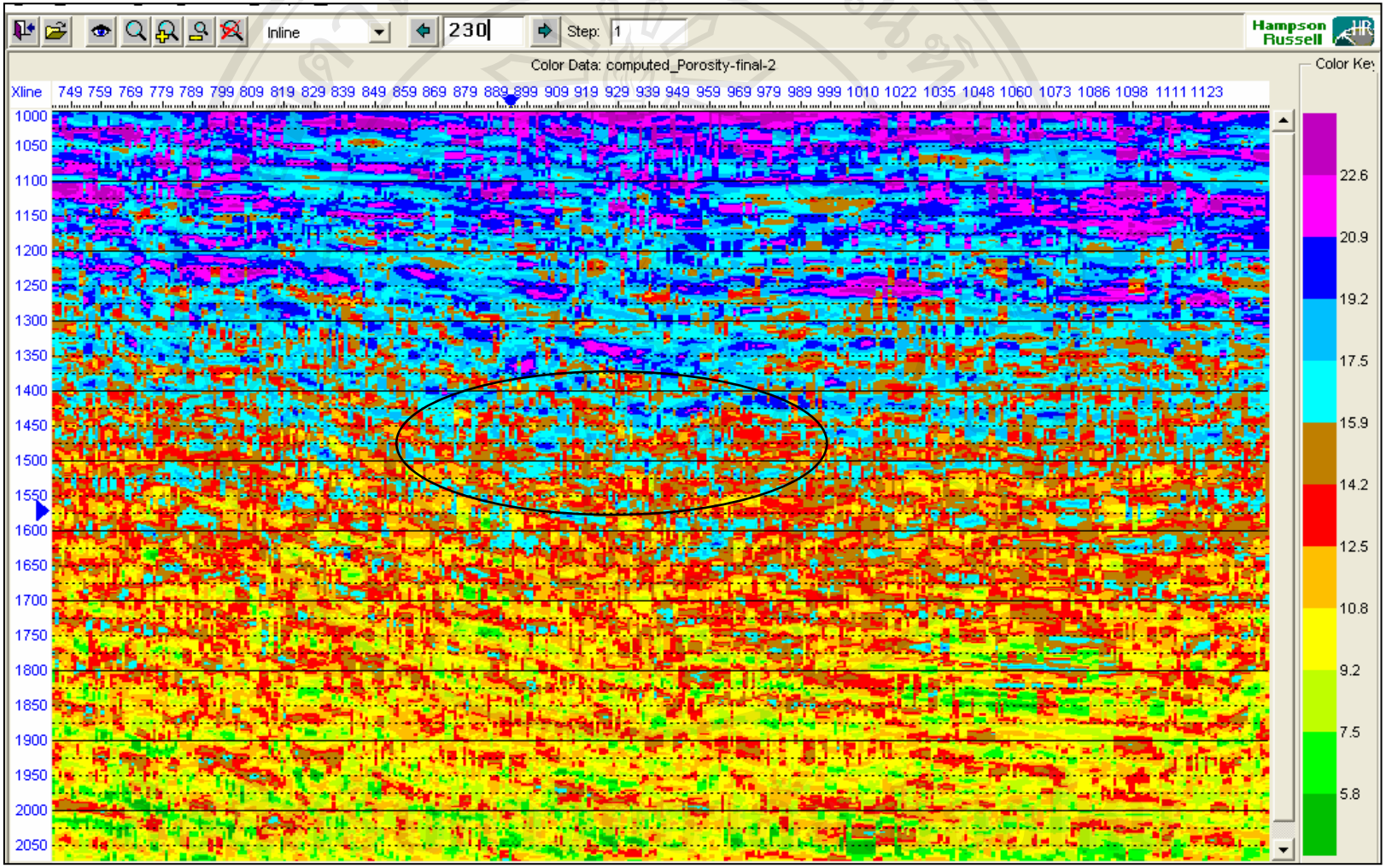

Figure 3.27 Inline 230 from predicted porosity volume.

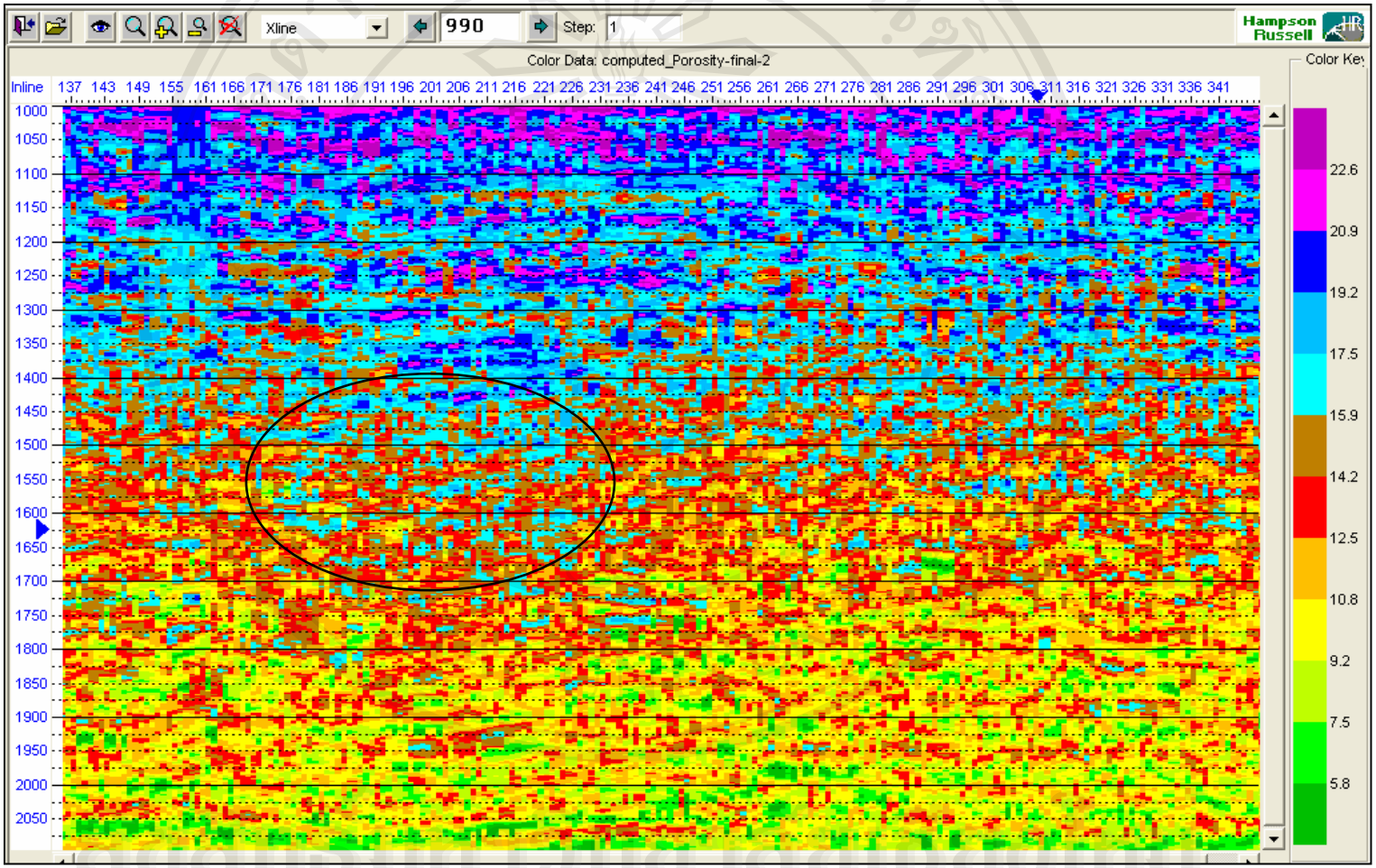

Figure 3.28 Cross line 990 from predicted porosity volume.

The slice at 1400 milliseconds shows some features that can be interpreted as meandering/braided channels. The blue and pink colors indicate relatively higher porosity while the red and yellow colors indicate areas of relatively lower porosity.

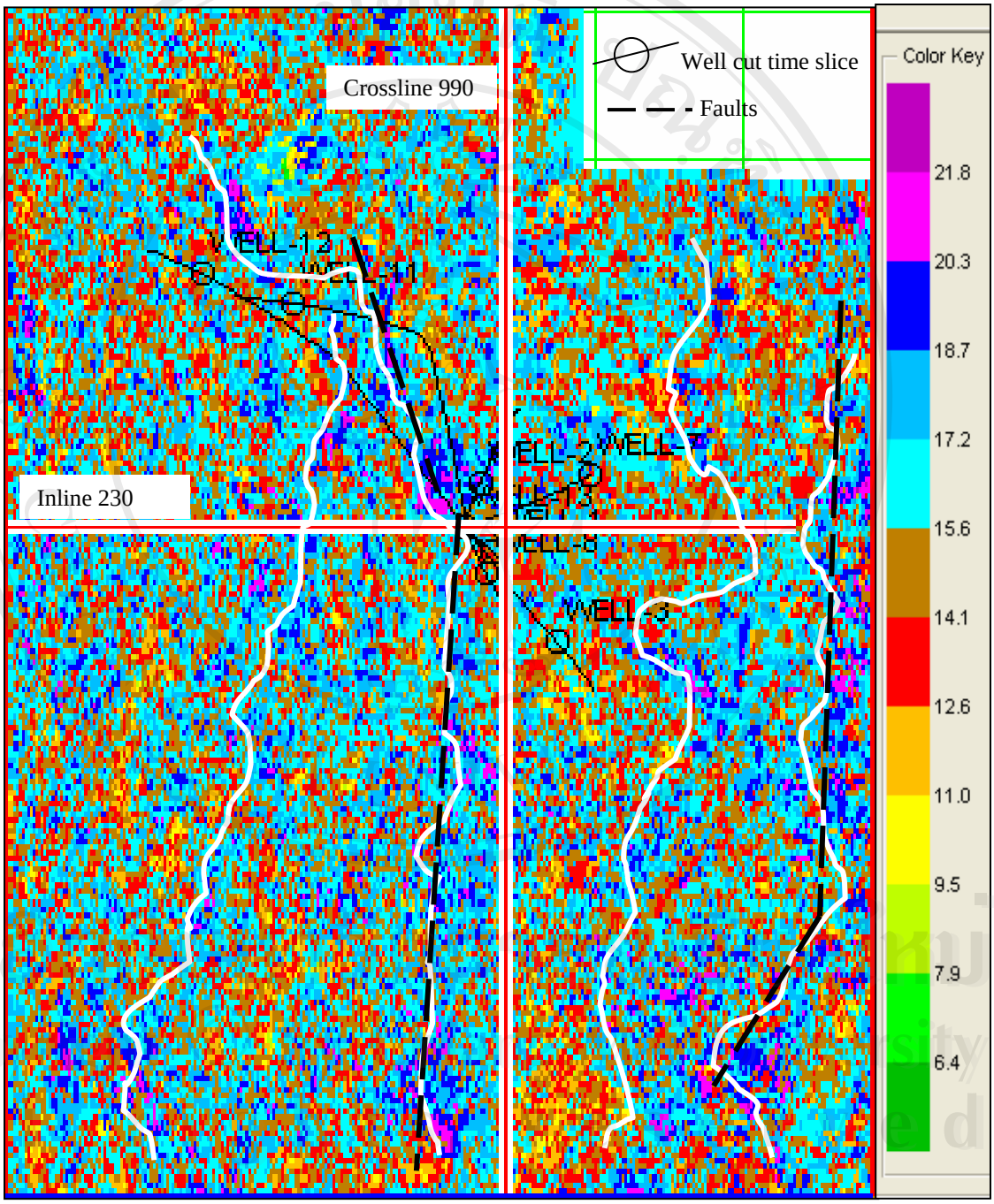

Figure 3.29 Time slice at 1400 milliseconds. White solid lines indicate the interpreted channel sands. Black dashed lines are faults interpreted by Bundarnsin, T., 2006.

In Figure 3.29, the white curved lines, which were interpreted as following higher porosity trends, reflecting a pattern of channels running north-south. The white lines were drawn to follow the trend only, these lines do not imply the channel boundary. Since these trends are not very clear, time slices above and below the target sandstone layers were also interpreted to reveal more features. Figures 3.30 and 3.31 are time slices above the target sandstone layers at 1300 and 1350 milliseconds, respectively. In these figures the channel features are more visible. Figures 3.32 and 3.33 are time slices below the target sandstone layer at 1450 and 1500 milliseconds, respectively. On these slices, the channels are wider. However, a deeper slice at 1800 milliseconds (Figure 3.34) also indicates the presence of these relatively higher porosity channel-like features. The time slices have been interpreted as showing the relative distribution of higher and lower porosity and not the absolute predicted porosity value.

The other possible interpretation of these high porosity trends might be due to the juxtaposition of deeper low porosity rocks and younger high porosity rocks as a result of normal faulting. In a rift basin like Pattani basin it is common to have normal faults which can also give sharp porosity variation in a time slice. Bundarnsin, T.(2006), also interpreted some major faults in the study area.

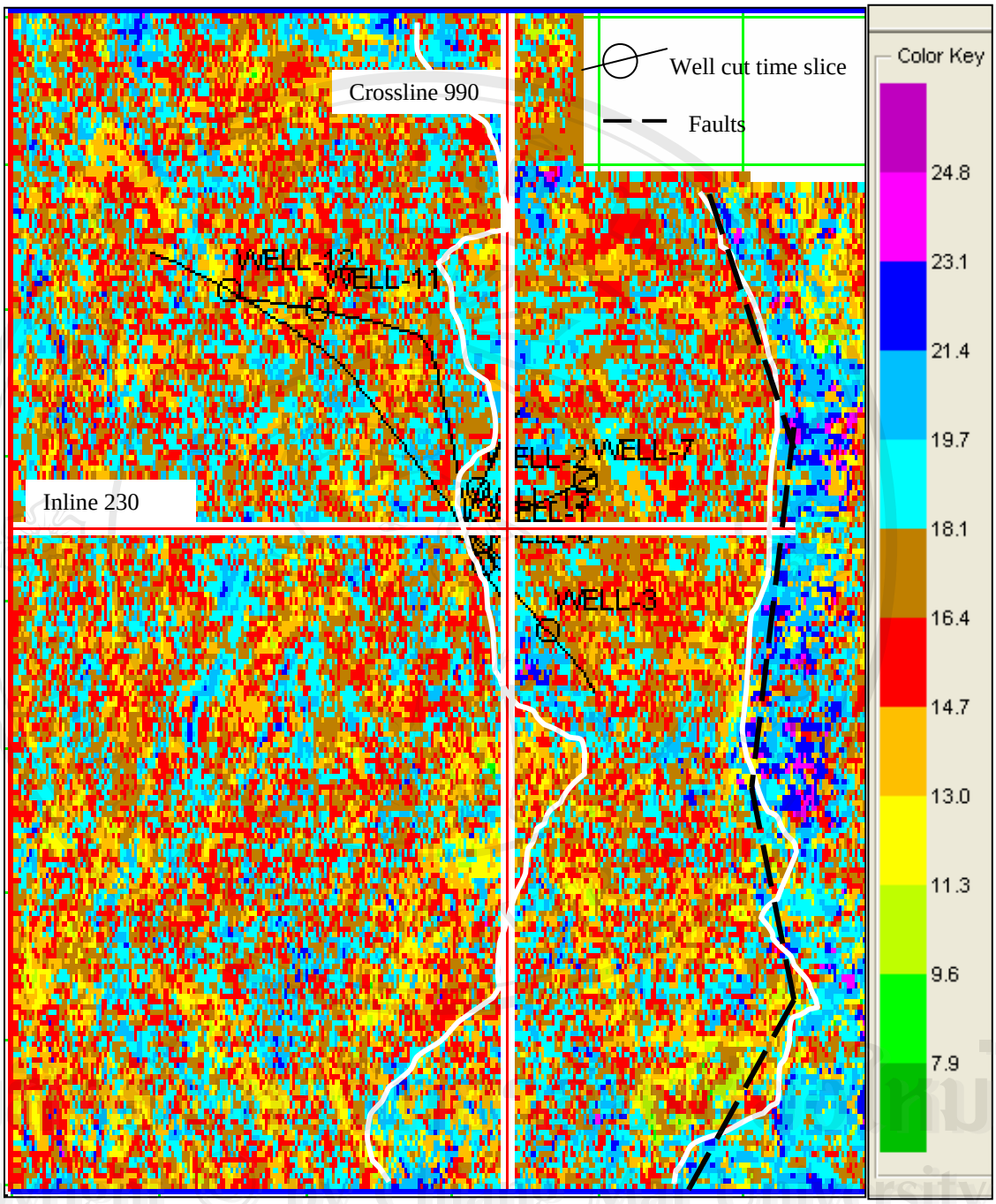

Figure 3.30 Time slice at 1300 milliseconds. White solid lines indicate the interpreted channel sands. Black dashed lines are faults interpreted by Bundarnsin, T., 2006.

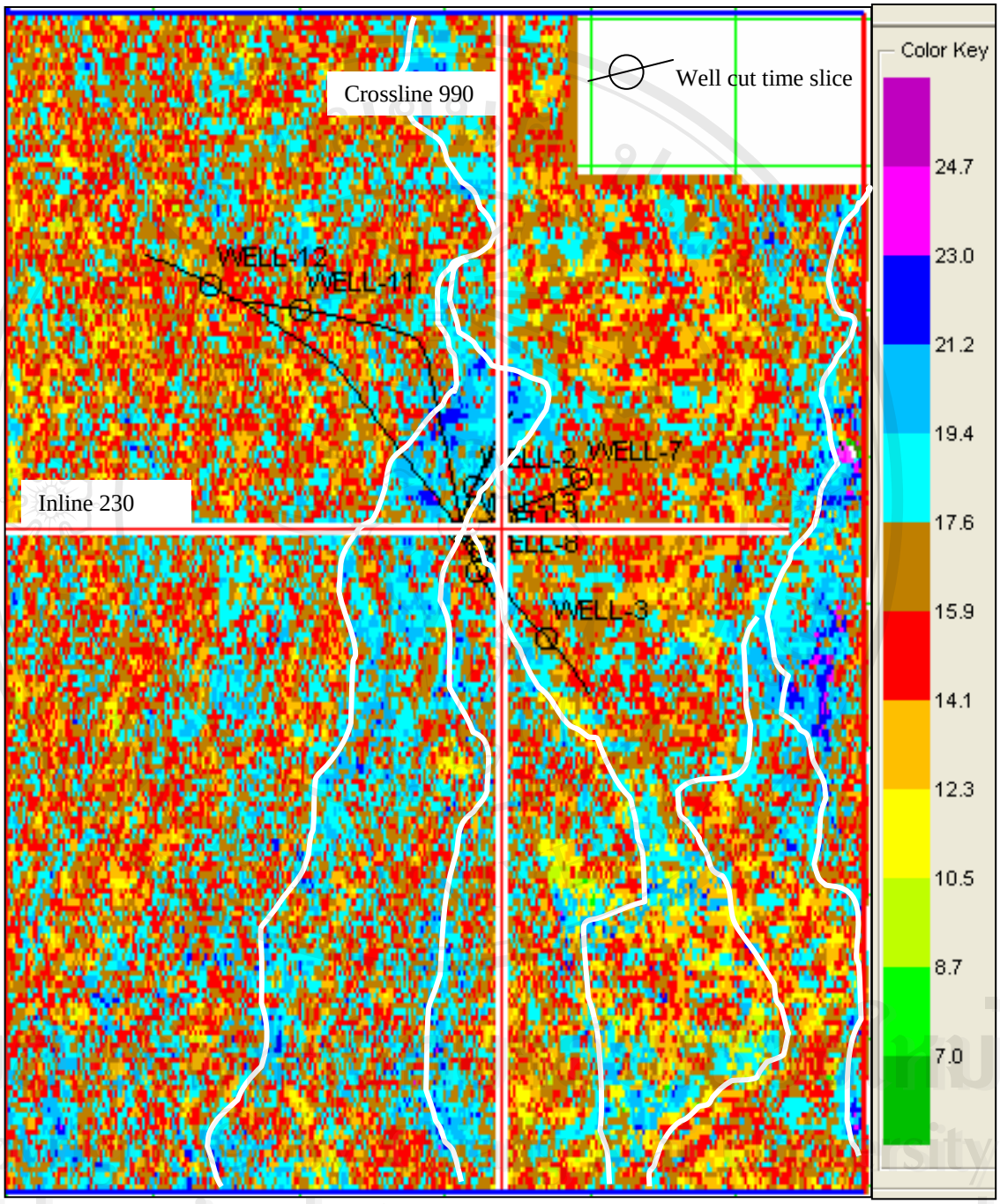

Figure 3.31 Time slice at 1350 milliseconds. White solid lines indicate the interpreted channel sands.

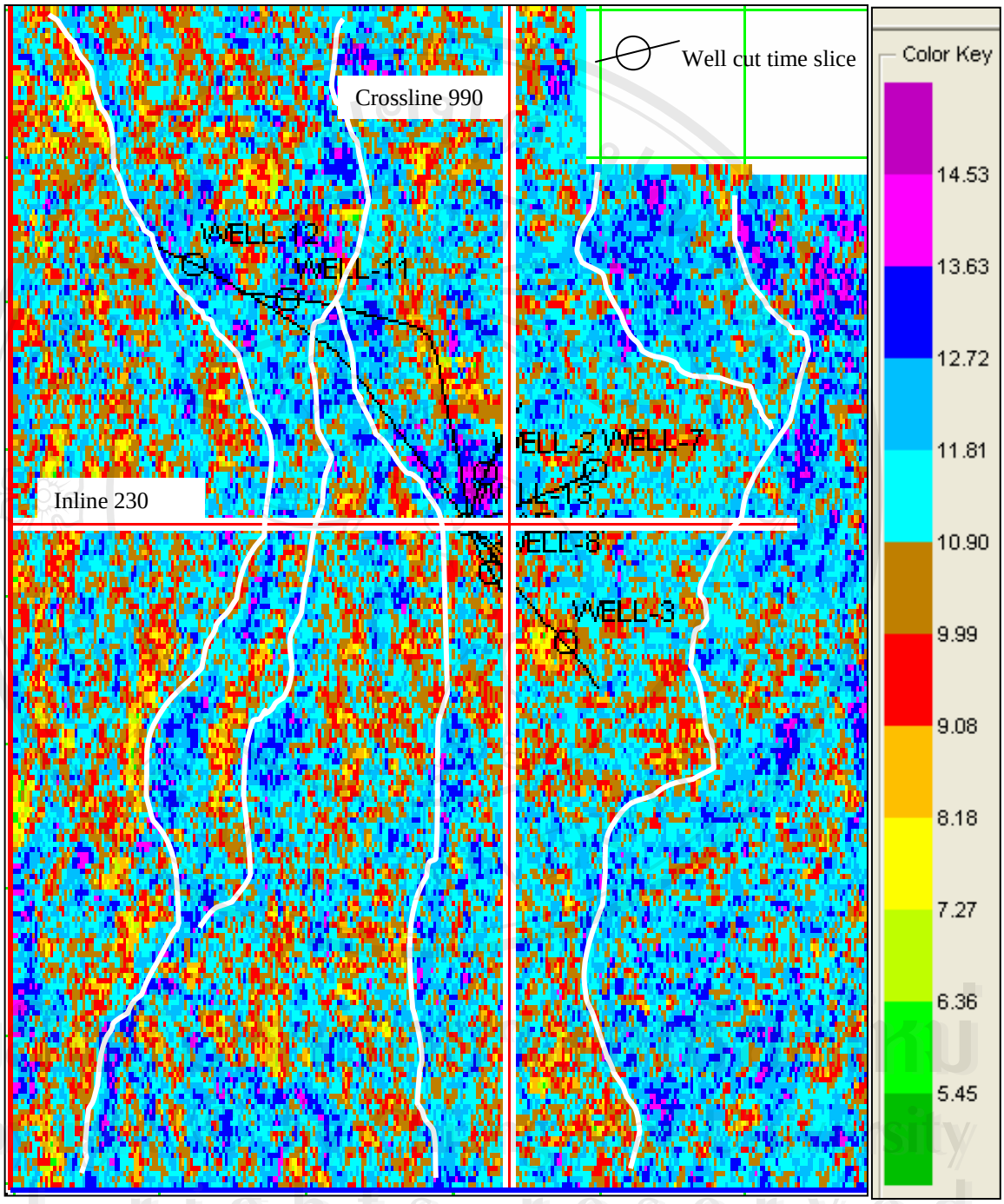

Figure 3.32 Time slice at 1450 milliseconds. White solid lines indicate the interpreted channel sands.

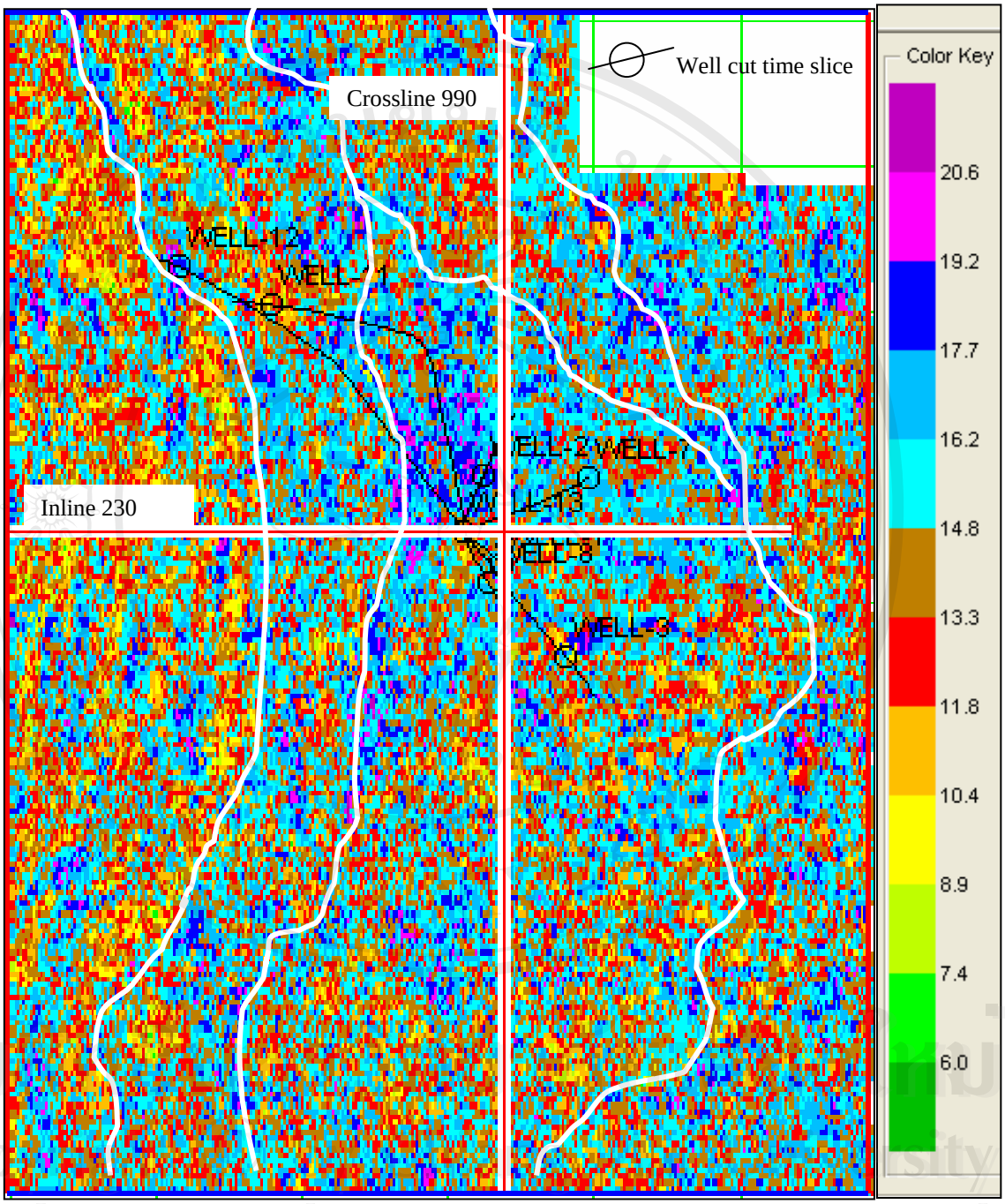

Figure 3.33 Time slice at 1500 milliseconds. White solid lines indicate the interpreted channel sands.

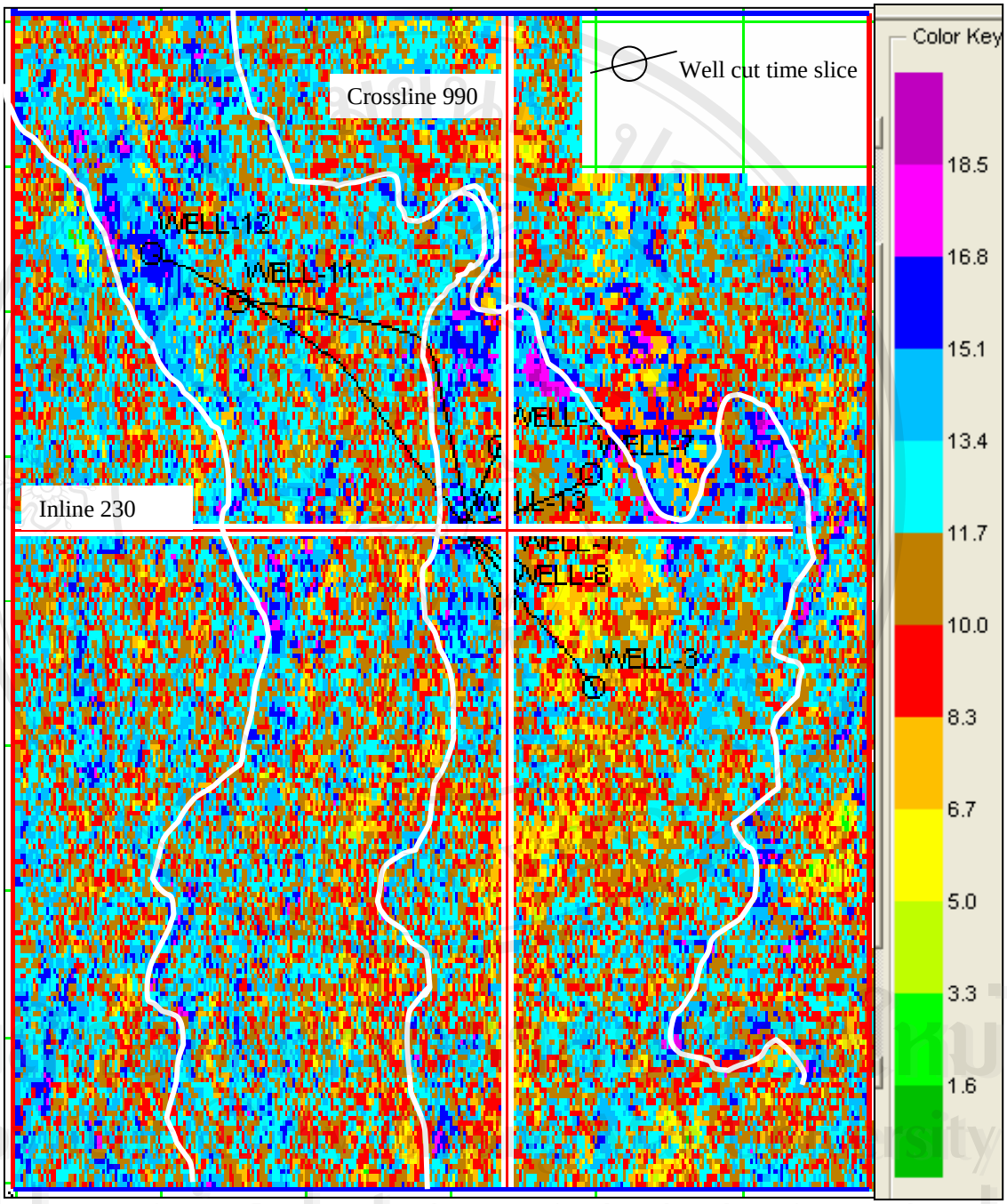

Figure 3.34 Time slice at 1800 milliseconds. White solid lines indicate the interpreted channel sands.